DALTON
FULL PAPER

High-nuclearity palladium carbonyl trimethylphosphine clusters containing unprecedented face-condensed icosahedral-based transition-metal core geometries: proposed growth patterns from a centered Pd_{13} icosahedron †

Nguyet T. Tran, Masaki Kawano and Lawrence F. Dahl *

Department of Chemistry, University of Wisconsin-Madison, Madison, WI 53706, USA. E-mail: dahl@chem.wisc.edu

Received 19th April 2001, Accepted 21st June 2001
First published as an Advance Article on the web 17th September 2001

The preparation, isolation, and structural/bonding characterization of four high-nuclearity neutral homopalladium clusters, $Pd_{16}(CO)_{13}(PMe_3)_9$ **1**, $Pd_{35}(CO)_{23}(PMe_3)_{15}$ **2**, $Pd_{39}(CO)_{23}(PMe_3)_{16}$ **3** and $Pd_{59}(CO)_{32}(PMe_3)_{21}$ **4**, and a minor bimetallic product, $Pd_{29}Ni_3(CO)_{22}(PMe_3)_{13}$ **5**, are given. The four homopalladium clusters were characterized by CCD X-ray crystallographic determinations, elemental analyses, IR, multinuclear NMR, and cyclic voltammetry; because **5** was obtained in very low yields, both its molecular geometry and composition were established from the X-ray crystallographic analysis. These five clusters, obtained from reactions of a ccp Pd–Ni carbonyl cluster precursor and PMe_3 (with or without acetic acid), exhibit five different types (four unprecedented) of centered icosahedral-based transition-metal frameworks: (1) the Pd_{16} core in **1** possesses a centered Pd_{13} icosahedron. (2) The Pd_{35} and Pd_{39} cores in **2** and **3** each have a face-fused centered Pd_{23} biicosahedron with linear (pseudo-D_{3h}) and bent (pseudo-C_{2v}) geometries, respectively; the pseudo-D_{3h} central Pd_{29} polyhedron of the Pd_{35} core in **2** approximately conforms to *five* interpenetrating centered icosahedra. (3) The crystallographic-D_3 (32) Pd_{59} core in **4** has two centered Pd_{13} icosahedra that are *indirectly* connected *via trans* double face-sharing with an inner face-fused Pd_9 bioctahedron; the entire nanosized face-condensed Pd_{59} core has 11 interior Pd(i) atoms. (4) The $Pd_{29}Ni_3$ core in **5** contains a pseudo-T_d central Pd_{26} polyhedron comprised of *four* interpenetrating centered icosahedra. The existence of these highly condensed icosahedral-based metal carbonyl clusters, found only for Pd but not for the other eight Group 8–10 transition metals, may be ascribed to Pd metal having the weakest metal–metal bonding (*i.e.*, smallest cohesive energy). Electronic closed-shell stabilization of each of these clusters is indicated by electron-counting condensation rules giving calculated values in exact agreement with observed electron counts for the metal cores in **1**, **2**, **4**, and **5** (*i.e.*, irregular condensations prevent a reliable electron count in **3**). Proposed growth sequences provide logical pathways in the formation of the central palladium fragments in **2**, **3**, **4** and **5** from the centered Pd_{13} icosahedral fragment in **1**.

Introduction

Extensive chemical/physical studies have been performed on high-nuclearity nickel and platinum carbonyl clusters (arbitrarily designated by us to possess a minimum of 10 metal atoms with direct metal–metal connectivities),[1,2] and (prior to last year) ones containing up to 50 metal atoms have been isolated and crystallographically characterized.[3] In sharp contrast, relatively few investigations involving palladium carbonyl clusters have been carried out, partly because palladium *per se* does not form stable, discrete homometallic carbonyl clusters at room temperature in either solid or solution states.[2,4–6] Nevertheless, solution-phase palladium carbonyl complexes have been synthesized with other stabilizing ligands (*e.g.*, phosphines),[7a,b] and carbon monoxide readily absorbs on palladium surfaces.[7c] Moreover, gas-phase $[Pd_3(CO)_n]^-$ anions ($n = 1, 6$) have been generated and their binding energies determined *via* the collision-induced dissociation method.[7d]

$Pd_3(\mu_2\text{-}CO)_3(PPh_3)_4$[8] is the first known palladium carbonyl phosphine cluster, initially synthesized in 1969 *via* the reduction of $Pd(acac)_2$ by CO in the presence of PPh_3 and $AlEt_3$;[8a] its proposed molecular geometry was subsequently ascertained from an X-ray crystallographic determination.[8d] Since then, a considerable number of intriguing palladium carbonyl phosphine clusters have been prepared and their stereochemistry extensively investigated; however, the number of high-nuclearity homopalladium carbonyl clusters characterized by X-ray diffraction analysis is still limited: namely, $Pd_{10}(CO)_{14}(PBu^n_3)_4$,[9] $Pd_{10}(CO)_{12}(PBu^n_3)_6$,[10] $Pd_{12}(CO)_{12}(PBu^n_3)_6$,[11] $Pd_{16}(CO)_{13}(PEt_3)_9$,[12] $Pd_{23}(CO)_{22}(PEt_3)_{10}$,[13] $Pd_{23}(CO)_{20}(PEt_3)_8$,[14] $Pd_{34}(CO)_{24}(PEt_3)_{12}$,[15] and $Pd_{38}(CO)_{28}(PEt_3)_{12}$.[15,16] These eight palladium carbonyl phosphine clusters were prepared over the last 20 years by Mednikov and coworkers and structurally characterized by Slovokhotov and Struchkov from X-ray crystallography. Analyses of the geometries and prominent bonding features of several of these clusters have been reported.[17] Synthetic pathways to these large clusters usually involve the elimination of ligands from smaller palladium clusters thereby resulting in aggregation to larger clusters. In general, the products of such reactions are unpredictable, and consequently X-ray crystallography is normally utilized to establish the composition as well as atomic arrangement. Recently we reported[18] an astonishing nanosized $Pd_{145}(CO)_x(PEt_3)_{30}$ cluster containing a capped three-shell 145-atom metal core of pseudo-I_h icosahedral symmetry.

Of relevance are the giant non-crystalline N,O-ligated nano-

† Dedicated to Professor Jack Lewis for his inspiring leadership and many seminal achievements in metal carbonyl cluster chemistry during his illustrious academic career at Cambridge University.

sized palladium clusters possessing idealized formulations based upon concentric closed-shell metal cores:[19] namely, 5-shell Pd_{561} clusters prepared by Moiseev and coworkers[20] and by Schmid *et al.*,[21] and mixtures of 7-shell Pd_{1415} and 8-shell Pd_{2057} clusters prepared by Schmid *et al.*[22] Chaudret, Bradley and coworkers[23] showed that zerovalent Pd (and likewise Pt) complexes in organic solutions (*e.g.*, THF) decompose under CO in the presence of PPh_3 to give PPh_3/CO-stabilized Pd (and Pt) nanosized particles that were investigated by spectroscopic methods; although the Pd particles were much less stable than the Pt particles and were subject to size variations in solution, three distinct size-selected distributions were obtained with observed mean diameters determined from TEM indicating idealized 2-shell Pd_{55}, 3-shell Pd_{147}, and 5-shell Pd_{561} cores.[23]

This paper presents the preparation, isolation, and structural determinations of several new high-nuclearity homopalladium carbonyl clusters: namely, $Pd_{16}(CO)_{13}(PMe_3)_9$ **1**, $Pd_{35}(CO)_{23}(PMe_3)_{15}$ **2**, $Pd_{39}(CO)_{23}(PMe_3)_{16}$ **3** and $Pd_{59}(CO)_{32}(PMe_3)_{21}$ **4**. These neutral palladium carbonyl trimethylphosphine clusters were obtained in moderate yields from a highly reproducible synthesis involving the initial preparation of a heterometallic Pd–Ni carbonyl cluster **A** (without phosphine ligands)[24] followed by its reaction with PMe_3 under acidic conditions. Although it was initially hoped that the latter reaction would result in a phosphine-stabilized derivative of **A** *via* PMe_3 substitution for CO ligands, the reaction instead gave rise to the above-mentioned four new high-nuclearity homopalladium clusters. The bimetallic Pd–Ni cluster, $Pd_{29}Ni_3(CO)_{22}(PMe_3)_{13}$ **5**, was obtained as a minor product along with **1** as the major product from the reaction of **A** with PMe_3 in the absence of acetic acid. A preliminary account of the synthesis and structural analysis of $Pd_{59}(CO)_{32}(PMe_3)_{21}$ **4** has been reported.[25]

One major outcome of this study is that the stoichiometries and geometries for four of the five palladium and palladium–nickel trimethylphosphine carbonyl clusters (**2**, **3**, **4** and **5**) are completely different from those containing PEt_3 and PBu^n_3 ligands previously reported by Mednikov, Slovokotov, Struchkov and coworkers[9–16] (*vide supra*); the one exception is the stoichiometrically and geometrically analogous $Pd_{16}(CO)_{13}(PR_3)_9$ clusters (R = Me **1**, Et[12]) which consist of a centered Pd_{13} icosahedron with three edge-bridged exopolyhedral μ_2-Pd(PR_3) fragments. This general dissimilarity in composition (and structure) may be attributed to markedly decreased steric effects of the phosphine-attached methyl substituents, as reflected by the significantly smaller Tolman PMe_3 cone angle θ (118°) *versus* those of 132 and 130° for the more bulky PEt_3 and PBu^n_3 ligands, respectively.[26] Because the five clusters presented herein were obtained *via* a completely different chemical route, kinetic factors may also be responsible for the different compositions of the isolated products.

Of comparable importance are the structural/bonding implications obtained from electron-counting analyses of the face-condensed icosahedral-based **2**, **4** and **5** and of the centered Pd_{13} icosahedron in **1** *versus* centered coinage-metal monoicosahedra and the Teo/Zhang vertex-sharing coinage-metal polyicosahedra. Proposed growth patterns are also presented for the formation of the central palladium fragments in **2**, **3**, **4** and **5** from the centered Pd_{13} icosahedral fragment in **1**.

Results and discussion

Structural/bonding features of $Pd_{16}(CO)_{13}(PMe_3)_9$ 1, $Pd_{35}(CO)_{23}(PMe_3)_{15}$ 2, $Pd_{39}(CO)_{23}(PMe_3)_{16}$ 3, $Pd_{59}(CO)_{32}(PMe_3)_{21}$ 4 and $Pd_{29}Ni_3(CO)_{22}(PMe_3)_{13}$ 5

(a) $Pd_{16}(CO)_{13}(PMe_3)_9$ 1. The configuration of **1** is presented in Fig. 1, and mean distances with corresponding ranges of individual distances are given in Table 1. Its Pd_{16} architecture of crystallographic C_3 symmetry consists of a centered icosahedral Pd_{13} core and three exopolyhedral μ_2-Pd(PMe_3) fragments that

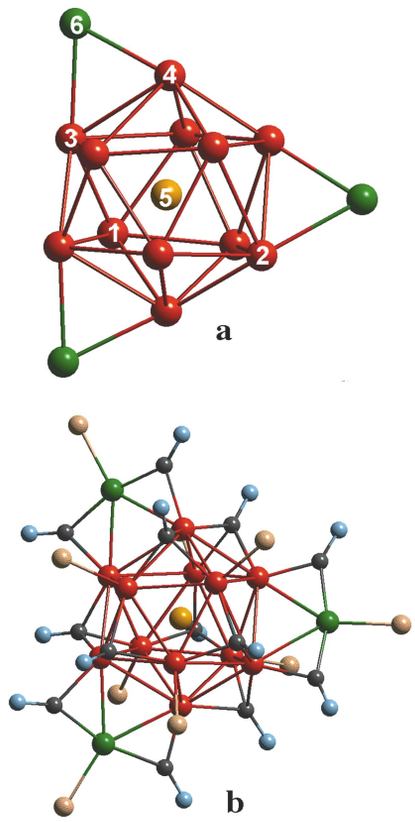

Fig. 1 (a) View of the Pd_{16} core-geometry in neutral $Pd_{16}(CO)_{13}(PMe_3)_9$ **1** showing the interior Pd(i) atom (gold) surrounded by 12 icosahedral Pd(cage) atoms (red) with three additional exopolyhedral edge-condensed capping Pd(c) atoms (green). (b) Configuration of **1**, which has crystallographic C_3 site symmetry, without the phosphorus-attached methyl substituents. The threefold axis passes through the icosahedral-centered Pd(i) atom and one triply bridging CO. Each of the edge-bridged exopolyhedral Pd(c) atoms ideally has a trigonal-planar ligand coordination of one PMe_3 and two doubly bridging COs. The entire Pd_{16} core is electronically/sterically stabilized by the surrounding nine PMe_3 and 13 bridging carbonyl ligands.

edge-bridge three pairs of adjacent Pd(cage) atoms within the Pd_{13} icosahedron. Six PMe_3 ligands are each coordinated to one of the other six Pd(cage) atoms. **1** is also ligated by 13 bridging CO ligands, of which seven are triply bridging and six doubly bridging. The crystallographic threefold axis passes through the interior Pd(i) atom and one triply bridging CO. Three triply bridging COs cap icosahedral Pd_3 triangular faces composed of one Pd(PMe_3) and two Pd(cage) atoms, while the other three triply bridging COs cap icosahedral Pd_3 triangular faces composed of one Pd(cage) and two Pd(PMe_3). The six doubly bridging COs link the three exopolyhedral μ_2-Pd(PMe_3) fragments to their connected palladium atoms such that each exopolyhedral Pd atom ideally has a trigonal-planar ligand arrangement.

1 is the trimethylphosphine analogue of the structurally determined brown $Pd_{16}(CO)_{13}(PEt_3)_9$,[12] which was formed from reactions of either $Pd_4(CO)_5(PEt_3)_4$ or $Pd_{10}(CO)_{12}(PEt_3)_6$ with $Me_3NO{\cdot}2H_2O$ in the presence of HOAc or Me_3N, respectively. A comparison of the molecular parameters of **1** (Table 1) with those of $Pd_{16}(CO)_{13}(PEt)_9$[12] reveals that the corresponding means and their dispersions are almost identical. Noteworthy is that for **1** the mean *radial* distance (2.74 Å) from the central Pd(i) atom to the 12 Pd(cage) atoms is significantly shorter than the mean *tangential* distance (2.88 Å) corresponding to the 30 icosahedral edges of the 12 Pd(cage) atoms. The experimentally determined *radial* compression of 4.9% {*i.e.*, [(2.88 Å − 2.74 Å)/2.88 Å] × 100} compares favorably with the predicted value of *ca.* 5% for a geometrically regular centered icosahedron.[27,28] **1** and its triethylphosphine

Table 1 Mean connectivities and corresponding individual ranges for $Pd_{16}(CO)_{13}(PMe_3)_9$ **1** [a, b]

Pd–Pd connectivities	N [c]	Mean/Å	Range/Å
Icosahedral radial edges Pd(i)–Pd(cage)	12	2.74	2.703(1)–2.789(1)
Icosahedral tangential edges Pd(cage)–Pd(cage)	30	2.88	2.763(1)–3.053(1)
Pd(c)–Pd(cage)	6	2.70	2.687(1)–2.716(1)
Pd(s)–Pd(s)	36	2.85	2.687(1)–3.053(1)
Other bonds			
Pd–μ_2-CO	12	2.03	1.995(11)–2.074(10)
Pd–μ_3-CO	21	2.13	2.086(9)–2.186(11)
Pd–P	9	2.31	2.309(3)–2.324(2)

[a] Pd_{16} core possesses crystallographic C_3 symmetry. [b] Pd(i) denotes the centered (interior) icosahedral atom, Pd(cage) the 12 icosahedral cage atoms, Pd(c) the three edge-bridged capping atoms, and Pd(s) all 15 surface atoms (including the 12 Pd(cage) and three Pd(c) atoms). [c] N denotes the number of individual connectivities for a given mean.

Table 2 Mean connectivities and corresponding individual ranges for $Pd_{35}(CO)_{23}(PMe_3)_{15}$ **2** [a, b]

Pd–Pd connectivities	N [c]	Mean/Å	Range/Å
Icosahedron with Pd(13) center			
Radial edges Pd(i)–Pd(cage)	12	2.72	2.644(4)–2.818(4)
Tangential edges Pd(cage)–Pd(cage)	30	2.86	2.641(4)–3.117(4)
Icosahedron with Pd(23) center			
Radial edges	12	2.73	2.597(4)–2.947(4)
Tangential edges	30	2.87	2.641(4)–3.260(4)
Icosahedron with Pd(1) center			
Radial edges	12	2.73	2.602(3)–2.942(4)
Tangential edges	30	2.87	2.597(4)–3.467(4)
Icosahedron with Pd(2) center			
Radial edges	12	2.73	2.603(3)–2.951(4)
Tangential edges	30	2.88	2.597(4)–3.551(4)
Icosahedron with Pd(3) center			
Radial edges	12	2.73	2.597(4)–2.960(4)
Tangential edges	30	2.88	2.603(3)–3.538(4)
Pd(c)–Pd(cage)	21	2.82	2.672(4)–3.102(4)
Pd(i)–Pd(i), axial–equatorial	6	2.63	2.597(4)–2.655(4)
Pd(i)–Pd(i), equat.–equat.	3	2.65	2.641(4)–2.664(4)
Pd(i)–Pd(cage)	42	2.77	2.610(4)–2.959(4)
Pd(s)–Pd(s)	87	2.92	2.703(4)–3.551(4)
Other bonds			
Pd–μ_2-CO	30	2.04	1.89(4)–2.15(4)
Pd–μ_3-CO	24	2.13	1.98(4)–2.39(4)
Pd–P	15	2.31	2.289(9)–2.328(10)

[a] Pd_{35} core possesses pseudo-C_3 symmetry. [b] Pd(i) denotes the five centered trigonal bipyramidal interior atoms, Pd(cage) the 24 icosahedral cage atoms for the five interpenetrating icosahedra, Pd(c) the remaining six face-condensed capping atoms, and Pd(s) all 30 surface atoms. [c] N denotes the number of individual connectivities for a given mean.

analogue are one of the two reported examples of a transition metal carbonyl cluster containing an all-metal complete centered icosahedron. The other example (to our knowledge) is the $[Au_2Pd_{14}(\mu_2\text{-}CO)_2(\mu_3\text{-}CO)_7(PMe_3)_4]^{2+}$ dication ($[PF_6]^-$ salt), prepared and structurally characterized by Mingos and co-workers,[29] which possesses a Pd-centered Au_2Pd_{10} icosahedral cage that shares a common edge with a Pd_5 trigonal bipyramid.

(b) $Pd_{35}(CO)_{23}(PMe_3)_{15}$ 2. The configuration of **2** is given in Fig. 2, and mean distances with corresponding ranges of individual distances are presented in Table 2. The X-ray structural determination showed that the Pd_{35} core-geometry, which has no crystallographically imposed symmetry but ideally conforms to C_3 symmetry, possesses a direct face-condensation of two centered Pd_{13} icosahedra that was heretofore unknown in transition-metal cluster chemistry. This face-fused Pd_{23} biicosahedron of pseudo-D_{3h} symmetry (also designated as a twinned icosahedron) is also linked by *three* additional intericosahedral bonding connectivities resulting from *three* threefold-related pairs of corresponding threefold-related Pd(cage) atoms in the two face-sharing icosahedra being positioned at analogous weakly bonding Pd–Pd distances [mean, 2.98 Å; range, 2.941(4)–3.020(4) Å]. The two icosahedral-centered Pd(i) atoms and the three Pd(i) atoms at the common face of the two Pd_{13} icosahedra form a nearly regular interior $Pd(i)_5$ trigonal bipyramid with a mean Pd(i)–Pd(i) distance of 2.64 Å [range, 2.597(4)–2.664(4) Å].

Further examination (Fig. 2) reveals that this pseudo-D_{3h} Pd_{23} biicosahedron and six additional face-condensed Pd atoms [*viz*., Pd(24), Pd(25), Pd(26), Pd(30), Pd(31), Pd(32)] may be envisioned as *five* interpenetrating centered icosahedra composed of the five Pd(i) and 24 Pd(cage) atoms. The three equatorial Pd(i) atoms of the internal $Pd(i)_5$ trigonal bipyramid comprise the centered sites of the three additional interpenetrating icosahedra. Although somewhat distorted, the resulting Pd_{29} fragment-geometry ideally maintains D_{3h} symmetry. This central Pd_{29} fragment may also be described in terms of *nine interpenetrating* Pd_{19} double icosahedra (DI) that are each oriented along one of the nine edges of the interior $Pd(i)_5$ trigonal bipyramid with the *common* seven-atom fragment of each DI being a pentagonal bipyramid. The six remaining capping Pd(c) atoms combine in a specific fashion with the central Pd_{29} fragment *via* further face-condensations to give the Pd_{35} core, such that the symmetry of the resulting *ideal* core-geometry is reduced from D_{3h} to C_3.

Although individual *radial* Pd(i)–Pd(cage) and *tangential* Pd(cage)–Pd(cage) distances within each of the five interpenetrating centered icosahedra comprising the Pd_{29} fragment in the Pd_{35} core of **2** vary greatly (Table 2), the ranges of the resulting five *radial* and five *tangential* means of 2.72–2.73 Å and

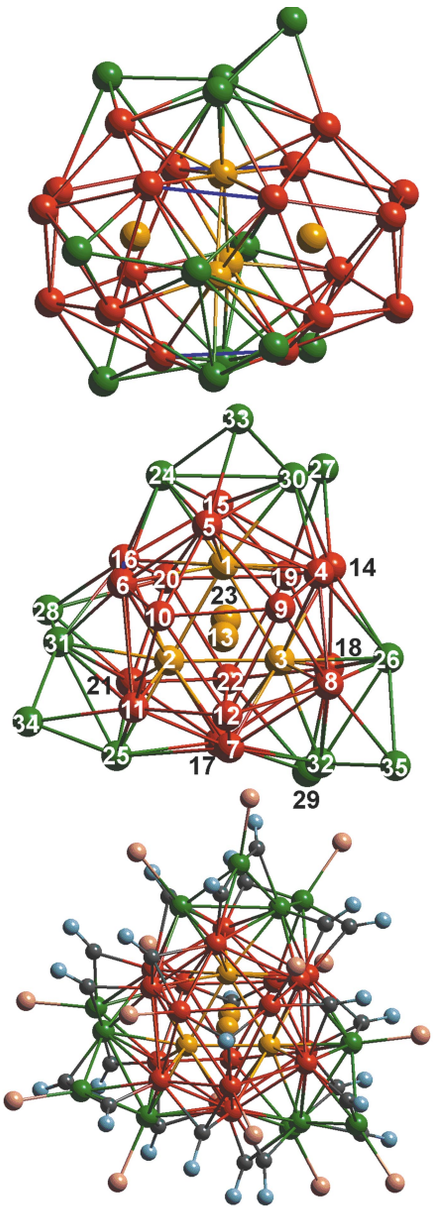

Fig. 2 (a) Side view of the Pd_{35} core-geometry of pseudo-C_3 symmetry in neutral $Pd_{35}(CO)_{23}(PMe_3)_{15}$ **2** showing a direct face-sharing condensation of two centered icosahedra (heretofore unknown in transition-metal cluster chemistry). This face-fused Pd_{23} biicosahedron has *three* additional threefold-related direct icosahedral Pd(cage)–Pd(cage) linkages; the two icosahedral-centered Pd(i) atoms (gold) and the three Pd(i) atoms (gold) of the common face-sharing triangle form a nearly regular, strongly bonding $Pd(i)_5$ trigonal bipyramid. This pseudo-D_{3h} Pd_{23} biicosahedron and six additional Pd(cage) atoms (red) may be envisioned as *five* interpenetrating centered icosahedra with the three trigonal-bipyramidal equatorial Pd(i) atoms being the centered sites of the three additional interpenetrating icosahedra. The resulting pseudo-D_{3h} central Pd_{29} fragment and the remaining six face-condensed capping Pd(c) atoms (green) form the Pd_{35} core in **2** of pseudo-C_3 symmetry. (b) Front view of the Pd_{35} core-geometry in **2** with atom labeling. The five interior Pd(i) atoms (gold) comprising a strongly bonding trigonal bipyramid, the other 18 Pd(cage) atoms (red) of the Pd_{23} face-fused biicosahedron, and six additional Pd atoms (red), (*viz.*, Pd(24), Pd(25), Pd(26), Pd(30), Pd(31), Pd(32)) approximately conform to a pseudo-D_{3h} Pd_{29} polyhedron composed of five interpenetrating icosahedra. Addition of the remaining six face-condensed capping Pd(c) atoms (green) lowers the symmetry to pseudo-C_3. (c) Configuration of **2**, which has pseudo-C_3 symmetry, without the phosphorus-attached methyl substituents. The entire Pd_{35} core is electronically/sterically stabilized by the encapsulating 15 PMe_3 and 23 bridging carbonyl ligands.

2.86–2.88 Å, respectively, are virtually identical and are completely consistent with the corresponding *radial* and *tangential* means determined for the Pd_{13} icosahedron in the Pd_{16} core of **1**.

2 is ligated by 15 PMe_3 and 15 doubly and eight triply bridging carbonyl ligands. The two triply bridging COs lying on the pseudo-C_3 axis are coordinated to the two outermost icosahedral triangular faces that are directly opposite to the common $Pd(i)_3$ triangular face of the face-fused Pd_{23} biicosahedron. Each of the six icosahedral Pd(cage) atoms in these two outermost icosahedral triangles is also bonded to a PMe_3 group. Of the other nine PMe_3 ligands, three are coordinated to three of the six Pd(cage) atoms that are face-condensed with the face-fused Pd_{23} biicosahedron to give the central interpenetrating Pd_{29} pentaicosahedron, while the other six are attached to the six capping Pd(c) atoms. The remaining six triply bridging COs each cap one of the six icosahedral triangular faces under pseudo-C_3 symmetry. Each of the six capping Pd(c) atoms has two doubly bridging COs that edge-bridge two of its connected icosahedral Pd(cage) atoms. The other three doubly bridging COs each edge-bridge two icosahedral Pd(cage) atoms.

(c) $Pd_{39}(CO)_{23}(PMe_3)_{16}$ 3. The configuration of **3** is presented in Fig. 3, and mean distances with corresponding ranges of individual distances are given in Table 3. This cluster has crystallographic C_2 site symmetry such that the independent atoms comprise one-half of the molecule. As found in $Pd_{35}(CO)_{23}(PMe_3)_{15}$ **2**, the molecular geometry of **3** also contains a face-fused Pd_{23} biicosahedral fragment (*i.e.*, a twinned icosahedron) with the two centered Pd(i) atoms of the two icosahedra and their three face-sharing Pd(i) atoms likewise forming an interior $Pd(i)_5$ trigonal bipyramid. However, in sharp contrast to the highly symmetrical Pd_{23} fragment-geometry in **2**, the corresponding Pd_{23} fragment-geometry in **3** is distorted from pseudo-D_{3h} symmetry *via* a large bending deformation (of ≈15°) about one of the three horizontal twofold axes (which then becomes the crystallographic twofold axis in **3**). This large pseudo-C_{2v} geometrical tipping of the two face-fused icosahedra from each other in **3** is evidenced by: (1) the two icosahedra being additionally connected by only *two* instead of *three* weakly bonding links: namely, two symmetry-equivalent Pd(3)–Pd(5) and Pd(3A)–Pd(5A) bonding connectivities of 2.954(4) Å (that are analogous to those in **2**) *cf.* the third intericosahedral Pd(6)–Pd6A nonbonding connectivity of 4.029(5) Å; and (2) the particular geometrical irregularity of the trigonal-bipyramidal $Pd(i)_5$ kernel having two short symmetry-equivalent Pd(1)–Pd(axial) bonds [2.556(3) Å] and seven longer ones [2.726(5)–2.814(4) Å]. This observed angular deformation in **3** is a consequence of the asymmetric face-condensations of the other 16 surface atoms about this face-fused Pd_{23} biicosahedron. One geometrical consequence is that the mean of the three intratriangular bond distances at the common Pd_3 triangular face between the two icosahedra is significantly shorter in **2** (2.65 Å) than in **3** (2.76 Å).

Although the individual *radial* Pd(i)–Pd(cage) and *tangential* Pd(cage)–Pd(cage) distances within the crystallographically independent icosahedron of **3** vary considerably (as also was found in **1** and **2**), their means of 2.73 and 2.87 Å, respectively, are analogous with those in both **1** and **2**; consequently, the experimentally determined radial compression of 4.9% is virtually identical with those found in **1** and **2** in accordance with the *average* distances of the deformed geometrical shape of each Pd_{13} icosahedron closely corresponding to those of a geometrically regular one. The relatively short Pd(i)–Pd(i) distances (mean, 2.74 Å) point to relatively strong bonding interactions within the trigonal bipyramidal $Pd(i)_5$ kernel. The 16 condensed Pd(c) atoms form 40 Pd(c)–Pd(i, cage) connectivities [mean, 2.84 Å, range 2.690(3)–3.257(4) Å] as a result of different condensation modes with unsymmetrical linkages.

3 is stabilized by 16 PMe_3 and 23 bridging CO ligands; the latter consist of 8 triply bridging and 15 doubly bridging ones. The crystallographically imposed twofold axis passes through

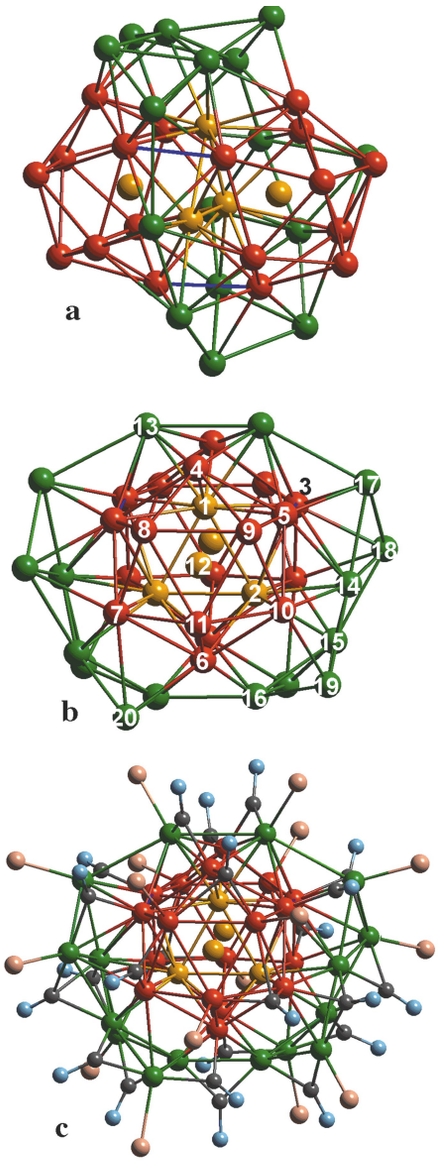

Fig. 3 (a) Side view of the Pd_{39} core-geometry of crystallographic C_2 site symmetry in neutral $Pd_{39}(CO)_{23}(PMe_3)_{16}$ **3** showing (as in **2**) a direct face-sharing condensation of two centered Pd_{23} icosahedra. Unlike **2**, there are only *two* (instead of *three*) additional intericosahedral bond-linkages due to a large bending deformation of the face-fused centered Pd_{23} biicosahedron (and its trigonal bipyramidal $Pd(i)_5$ kernel) from a pseudo-D_{3h} to a crystallographic C_2 geometry. This angular deformation is attributed to the observed asymmetric face-condensations of the other 16 Pd atoms to the central Pd_{23} fragment. (b) Front view of the Pd_{39} core-geometry in **3** with atom labeling. The crystallographic twofold axis passes through the equatorial Pd(1) atom (gold) and the midpoint of the two other equatorial atoms in the C_2-deformed $Pd(i)_5$ trigonal bipyramid. (c) Configuration of **3**, which has crystallographic C_2 site symmetry, without the phosphorus-attached methyl substituents. The entire Pd_{39} core is sterically protected by the surrounding 16 PMe_3 and 23 bridging carbonyl ligands.

Pd(1) and a doubly bridging CO at the central bottom part of the molecule. Six PMe_3 ligands are attached to the six Pd(cage) atoms of the two outer triangular faces of the Pd_{23} biicosahedron (opposite to their common face-fused triangular face).

(d) $Pd_{59}(CO)_{32}(PMe_3)_{21}$ 4. The configuration of **4** is given in Fig. 4, and mean distances with corresponding ranges of individual distances are furnished in Table 4. **4** has crystallographic D_3 site symmetry such that the asymmetric part of the Pd_{59} core consists of one-sixth of the neutral molecule. Its 59-atom metal framework may be conceptually constructed in the following fashion. Two outer centered icosahedra are *indirectly* connected *via trans* double face-sharing with an inner face-shared biocta-

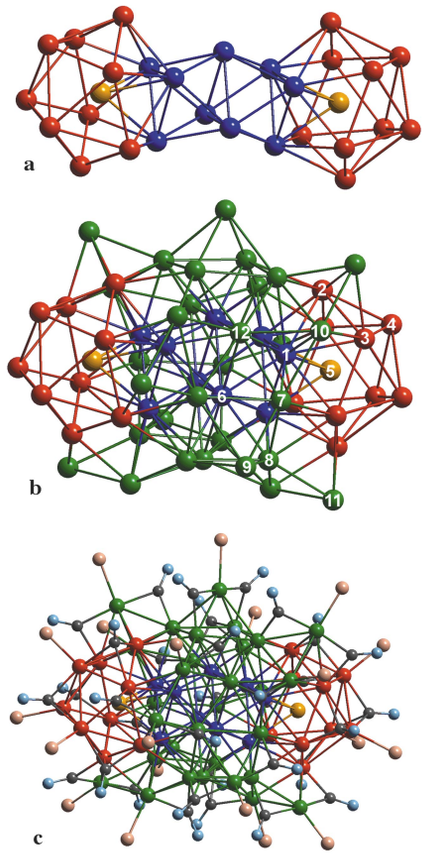

Fig. 4 (a) Side view of the central Pd_{29} part of the Pd_{59} core-geometry in neutral $Pd_{59}(CO)_{32}(PMe_3)_{21}$ **4** of crystallographic D_3 site symmetry showing an inner $Pd(i)_9$ bioctahedron (blue) that is face-fused to two outer centered Pd_{13} icosahedra. The 11 *interior* Pd(i) atoms consist of a bicapped face-fused bioctahedron. The principal threefold axis passes through the two icosahedral-centered Pd(i) atoms (gold) and the midpoints of the three perpendicular face-fused triangles (blue) interconnecting the two icosahedra and two octahedra with one another. Each of the three horizontal twofold axes passes through one of the three face-sharing bioctahedral Pd(i) atoms (blue) and the midpoint of the opposite triangular edge connecting the other two face-sharing Pd(i) atoms. (b) Side view of the ellipsoidal-shaped nanosized Pd_{59} core-geometry in **4**, which has a maximum core diameter of *ca.* 1.3 nm along the principal threefold axis and of 0.9 nm along each of the three horizontal twofold axes. The growth pattern of its Pd_{59} framework involves a remarkable specific combination of face-condensations of the central Pd_{29} fragment with octahedral and square-pyramidal polyhedra and three capping atoms. (c) Configuration of **4**, which has crystallographic D_3 symmetry, without the phosphorus-attached methyl substituents. The entire Pd_{59} core is electronically/sterically stabilized by the encapsulating 21 PMe_3 and 32 bridging carbonyl ligands.

hedron. The 11 interior Pd(i) atoms comprise the bicapped face-sharing bioctahedron. The principal threefold axis passes through the two icosahedral-centered Pd(5), Pd(5A) atoms and the midpoints of the three perpendicular face-fused triangles interconnecting the two icosahedra and two octahedra with one another. Each of the two icosahedra is further condensed *via* face-sharing with six other octahedra and three square pyramids. Of the 20 triangular faces comprising each centered Pd_{13} icosahedron, the 10 faces (including the end face) in its outer half are not connected to any condensed metal atoms; of the 10 faces in its inner half, seven are face-fused with octahedra (including the one face that is faced-fused with one end of the bioctahedron) and three with square pyramids that give rise to external square faces for the resulting condensed polyhedron.

Three additional threefold-related octahedra, each lying on a horizontal twofold axis that passes through two vertices, are each connected indirectly to both icosahedra *via* face-fusion of two of its twofold-related faces with two intermediate octahedra that in turn are each face-fused with an icosahedron. The

Table 3 Mean connectivities and corresponding individual ranges for $Pd_{39}(CO)_{23}(PMe_3)_{16}$ **3**[a,b]

Pd–Pd connectivities	N[c]	Mean/Å	Range/Å
Each of two crystallographically equivalent icosahedra			
Radial edges Pd(i)–Pd(cage)	12	2.73	2.556(3)–2.814(4)
Tangential edges Pd(cage)–Pd(cage)	30	2.87	2.686(3)–3.276(4)
Pd(c)–Pd(i, cage)	40	2.84	2.690(3)–3.257(4)
Pd(i)–Pd(i), axial–equat.	6	2.72	2.556(3)–2.814(4)
Pd(i)–Pd(i), equat.–equat.	3	2.76	2.726(4)–2.775(4)
Pd(i)–Pd(s)	42	2.81	2.654(4)–3.278(4)
Pd(s)–Pd(s)	98	2.86	2.688(4)–3.255(4)
Other bonds			
Pd–μ_2-CO	30	1.99	1.83(4)–2.14(7)
Pd–μ_3-CO	24	2.15	1.87(6)–2.48(6)
Pd–P	16	2.32	2.29(2)–2.38(3)

[a] Pd_{39} core possesses crystallographic C_2 symmetry. [b] Pd(i) designates the five trigonal bipyramidal interior atoms, Pd(cage) the 18 icosahedral cage atoms for the face-fused biicosahedra, Pd(c) the other 16 condensed capping atoms, and Pd(s) all 34 surface atoms. [c] N denotes the number of individual connectivities for a given mean.

Table 4 Mean connectivities and corresponding individual ranges for $Pd_{59}(CO)_{32}(PMe_3)_{21}$ **4**[a,b]

Pd–Pd connectivities	N[c]	Mean/Å	Range/Å
Each of two crystallographically equivalent icosahedra			
Radial edges Pd(i)–Pd(cage)	12	2.72	2.661(1)–2.809(1)
Tangential edges Pd(cage)–Pd(cage)	30	2.86	2.756(2)–3.101(2)
Octahedra and square pyramids	159	2.82	2.673(1)–3.101(2)
Pd(12)–Pd	30	2.79	2.740(1)–2.855(1)
Pd(i)–Pd(i)	27	2.73	2.673(1)–2.819(3)
Pd(i)–Pd(s)	78	2.79	2.661(1)–3.100(2)
Pd(s)–Pd(s)	132	2.83	2.719(2)–3.008(2)
Other bonds			
Pd–μ_2-CO	36	1.99	1.904(15)–2.069(14)
Pd–μ_3-CO	42	2.11	1.977(16)–2.216(18)
Pd–P	21	2.32	2.280(4)–2.338(5)

[a] Pd_{59} core possesses crystallographic D_3 symmetry. [b] Pd(i) designates the 11 interior atoms (including the two centered icosahedral atoms and the nine central face-fused bioctahedral atoms), Pd(cage) the 18 atoms for the two icosahedra, and Pd(s) all 48 surface atoms. [c] N denotes the number of individual connectivities for a given mean.

metal core is completed by three capping atoms [*viz.*, Pd(12) and its two threefold-related atoms], each located on a twofold axis and each connected to 10 Pd atoms that are disposed in a hemispherical-like array. Consequently, the entire Pd_{59} core of **4** can be formally derived from a specific face-sharing condensation of two icosahedra, 17 octahedra, and six square pyramids involving 56 Pd atoms that are additionally linked by three symmetry-equivalent Pd_{10}-capped Pd atoms.

Despite the large variations of the individual Pd–Pd distances [range, 2.661(1)–3.101(1) Å], which are also found in **1**, **2** and **3** and in other high-nuclearity homopalladium carbonyl phosphine clusters,[9–16] the following trends are significant: (1) The 11 *interior* Pd(i) and 48 *surface* Pd(s) atoms give rise to 27 Pd(i)–Pd(i) distances [mean, 2.73 Å; range, 2.673(1)–2.819(1) Å], 78 Pd(i)–Pd(s) distances [mean, 2.79 Å; range, 2.661(1)–3.100(1) Å] and 132 Pd(s)–Pd(s) distances [mean, 2.83 Å; range, 2.719(1)–3.008(1) Å]. The three means, which reflect relatively strong Pd(i)–Pd(i) bonding interactions, are within 0.1 Å of that found in ccp Pd metal (2.751 Å).[30] (2) The *radial* Pd(i)–Pd(cage) and *tangential* Pd(cage)–Pd(cage) means of 2.72 and 2.86 Å, respectively, for the centered icosahedron are analogous to those found in **1**, **2** and **3**; the markedly shorter Pd(i)–Pd(cage) distances reflect much stronger *radial* bonding interactions. (3) The relatively small variations in the Pd–Pd distances from the independent capping Pd(12) atom to its 10-connected Pd atoms [mean 2.79 Å; range, 2.740(1)–2.855(1) Å] are consistent with delocalized metal–metal bonding, as evidenced by the close similarity of the mean to that in ccp Pd metal. (4) The overall average Pd–Pd bond distance in the 17 octahedra and 6 square-pyramids of **4** is 2.82 Å [range 2.673(1)–3.101(2) Å], which is close to the corresponding means of 2.82 and 2.84 Å in the octahedral fragments of $Pd_{10}(CO)_{14}(PBu^n_3)_4$[9] and $Pd_{23}(CO)_{22}(PEt_3)_{10}$,[13] respectively.

The Pd_{59} architecture is stabilized by 32 bridging CO and 21 PMe_3 ligands. The trimethyl phosphine ligands are distributed about the metal core as six $Pd(\mu_3\text{-}CO)_2PMe_3$, nine $Pd(\mu_2\text{-}CO)_2PMe_3$ and six $Pd(\mu_3\text{-}CO)PMe_3$ moities. The 32 carbonyl ligands consist of 14 triply bridging and 18 doubly bridging COs. Two triply bridging COs are situated on the threefold axis and are coordinated to triangular Pd(cage) atoms at the two outer end faces of both icosahedra. Each of the three horizontal twofold axes, which are normal to the principal threefold axis, passes through two atoms [*viz.*, Pd(9), Pd(6); Pd(9A), Pd(6A); or Pd(9B), Pd(6B)] of an octahedron, and one of the three capping atoms [*viz.*, Pd(12), Pd(1D), or Pd(1I)] lying on the middle molecular plane.

(e) $Pd_{29}Ni_3(CO)_{22}(PMe_3)_{13}$ 5. Its geometry of crystallographic C_3 site symmetry is displayed in Fig. 5, and means with corresponding ranges of its molecular parameters are given in Table 5. The X-ray diffraction analysis revealed that 26 Pd atoms of the $Pd_{29}Ni_3$ core form *four* interpenetrating centered icosahedra, where each centered atom is one of the four interior Pd(i) atoms that form a bonding tetrahedral kernel. This central Pd_{26} framework possesses pseudo-T_d symmetry with the four threefold axes being coincident with the four localized threefold axes of the interior $Pd(i)_4$ tetrahedron; one of these four threefold axes is the crystallographic threefold axis for the entire $Pd_{29}Ni_3(CO)_{22}(PMe_3)_{13}$ molecule. Each of the *six* edges of the $Pd(i)_4$ tetrahedron corresponds to a pseudo-fivefold axis of a localized 19-atom interpenetrating 1 : 5 : 1 : 5 : 1 : 5 : 1 double icosahedron (DI). However, this remarkable cluster is best

Table 5 Mean connectivities and corresponding individual ranges for $Pd_{29}Ni_3(CO)_{22}(PMe_3)_{13}$ **5**[a,b]

M–M bonds	N[c]	Mean/Å	Range/Å
Each of three crystallographically equivalent icosahedra A			
Radial edges Pd(i)–Pd(cage)	12	2.71	2.537(2)–2.884(1)
Tangential edges Pd(cage)–Pd(cage)	30	2.67	2.537(2)–3.085(1)
One icosahedron B			
Radial edges Pd(i)–Pd(cage)	12	2.69	2.578(2)–2.841(1)
Tangential edges Pd(cage)–Pd(cage)	30	2.73	2.537(2)–3.074(1)
Pd(c)–Pd(cage)	12	2.83	2.699(1)–3.151(1)
Ni(c)–Pd(cage)	9	2.63	2.579(2)–2.703(2)
Pd(i)–Pd(i)	6	2.56	2.537(2)–2.578(2)
Pd(i)–Pd(cage)	36	2.75	2.578(2)–2.884(1)
Pd(s)–Pd(s)	72	2.89	2.670(1)–3.151(1)
Other bonds			
Pd–μ_2-CO	21	2.02	1.933(12)–2.071(14)
Pd–μ_3-CO	21	2.12	1.965(13)–2.428(18)
Ni–μ_2-CO	9	1.90	1.870(15)–1.926(13)
Pd–P	10	2.29	2.193(4)–2.315(3)
Ni–P	3	2.17	2.166(4)

[a] $Pd_{29}Ni_3$ core possesses crystallographic C_3 symmetry. [b] Pd(i) denotes the four centered tetrahedral interior atoms, Pd(cage) the 22 cage atoms of the central Pd_{26} polyhedron comprised of four interpenetrating centered icosahedra, Pd(c) and Ni(c) the three face-condensed capping palladium and capping nickel atoms, respectively, and Pd(s) all 25 palladium surface atoms. [c] N denotes the number of individual connectivities for a given mean.

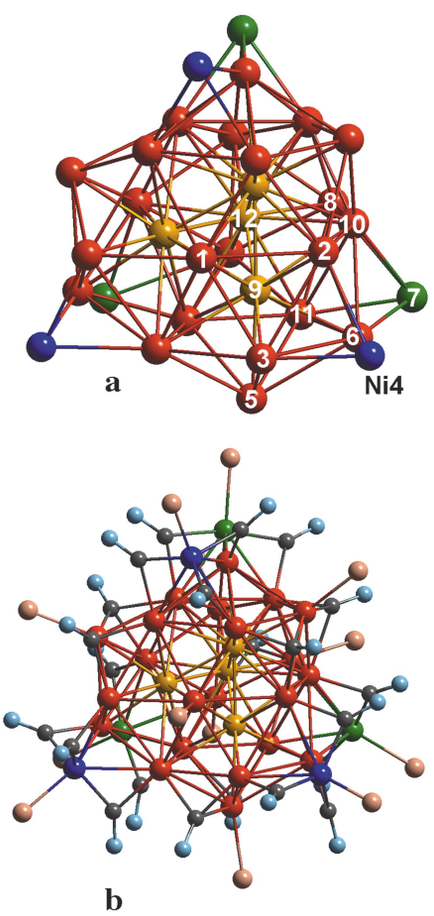

Fig. 5 (a) Front view of the neutral core-geometry of crystallographic C_3 site symmetry in neutral $Pd_{29}Ni_3(CO)_{22}(PMe_3)_{13}$ **5**. Its face-condensed $Pd_{29}Ni_3$ core contains a central Pd_{26} polyhedron of pseudo-T_d symmetry consisting of *four* interpenetrating centered icosahedra with the four icosahedral-centered interior Pd(i) atoms (gold) forming a strongly bonded tetrahedron that is encapsulated by 22 Pd(cage) atoms (red). The addition of three capping Pd(c) atoms (green) and three capping Ni(c) atoms (blue) to give the entire $Pd_{29}Ni_3$ core lowers the symmetry from T_d to crystallographic C_3. The threefold axis passes through the interior Pd(12) atom (gold) of the $Pd(i)_4$ tetrahedron, the Pd(cage) atom labeled Pd(1), and its attached phosphorus atom. (b) Configuration of **5**, which has crystallographic C_3 symmetry, without the phosphorus-attached methyl substituents. The entire $Pd_{29}Ni_3$ core is electronically/sterically stabilized by the surrounding 13 PMe_3 and 22 bridging carbonyl ligands.

considered as a Pd_{26} fragment that is created *via* the condensation of *four* centered icosahedra to give *four interpenetrating* icosahedra; the addition of three capping Ni and three capping Pd atoms to give the entire $Pd_{29}Ni_3$ core reduces the symmetry from T_d to crystallographic C_3.

Evidence that bonding interactions within the four interpenetrating centered icosahedra are strong is indicated by the relatively short Pd–Pd bond distances. The Pd(i)–Pd(i) connectivities among the four interior Pd(i) atoms comprising the tetrahedron are unusually short [mean, 2.56 Å; range, 2.537(2)–2.578(2) Å] compared to those within the interior $Pd(i)_4$ tetrahedron in the $Pd_{38}(CO)_{28}(PEt_3)_{12}$ cluster [mean, 2.70 Å; range, 2.514–2.958 Å].[15,16] For the three threefold-equivalent icosahedra A and the fourth icosahedron B lying on the crystallographic threefold axis, the mean *radial* Pd(i)–Pd(cage) connectivities are 2.71 and 2.69 Å, respectively, while the mean *tangential* Pd(cage)–Pd(cage) connectivities are 2.67 and 2.73 Å, respectively. These similar mean distances for the *radial* Pd(i)–Pd(cage) and *tangential* Pd(cage)–Pd(cage) connectivities in these four condensed icosahedra are a consequence of the *radial* bonds for one icosahedron being the *tangential* bonds for the other independent icosahedra, and *vice versa*. Connectivities involving the independent capping Pd(7) and Ni(4) atoms are within the normal bonding ranges: *viz.*, the means of 2.83 and 2.63 Å for the Pd(c)–Pd(cage), and Ni(c)–Pd(cage) distances, respectively, are comparable with 2.82 Å for the Pd(c)–Pd(cage) distances in $Pd_{35}(CO)_{23}(PMe_3)_{15}$ **2** and 2.84 Å for Pd(c)–Pd(i, cage) in $Pd_{39}(CO)_{23}(PMe_3)_{16}$ **3**. The shorter bonding distances in the central Pd_{26} fragment of $Pd_{29}Ni_3$ may be ascribed to the close packing of the 26 Pd atoms within the interpenetrating icosahedral arrangement.

The $Pd_{29}Ni_3$ core of **5** is stabilized by 13 PMe_3 and 22 CO ligands. The 22 carbonyl ligands are composed of seven triply bridging and 15 doubly bridging COs. The crystallographic threefold axis passes through Pd(1) and its attached PMe_3 ligand, the interior Pd(12), the midpoints of the interior Pd(9), Pd(9A), Pd(9B) and Pd(8), Pd(8A), Pd(8B) triangles, and the triply bridging CO attached to the Pd(8), Pd(8A), Pd(8B) triangle. The Pd(5) atom and its threefold-equivalent two Pd atoms each have one PMe_3 and two triply bridging COs. Each capping Ni atom is tetrahedrally coordinated to one PMe_3 and three doubly bridging CO ligands, while each of the three capping Pd(c) atoms is coordinated to the icosahedral fragment by one PMe_3 and two doubly bridging COs. The three remaining PMe_3 ligands are linked to the three Pd atoms of the bonding $[Pd(8)]_3$ triangle.

Application of cluster valence electron-counting models

(a) $Pd_{16}(CO)_{13}(PMe_3)_9$ 1. The observed electron count for **1** is (16 × 10) (Pd) + (13 × 2) (CO) + (9 × 2) (PMe_3) = 204 electrons. Application of the Mingos electron-counting approach [31] for the condensation of this centered icosahedron with three additional edge-bridging Pd atoms would give a valence electron count of 212 electrons [*i.e.*, (170 + 3) × 48 (triangle) − (3 × 34) (edge)) for $[Pd_{16}(CO)_{13}(PMe_3)_9]$ **1** under the assumption that the normal electron count for an icosahedron is 170.[32–38] However, Mingos [31] pointed out that for the case of a 13-atom centered icosahedron where *radial* bonding predominates (*i.e.*, with *tangential* surface bonding being negligible), the electron count is given by $12n_s + \Delta_i = (12 \times 12) + 18 = 162$ electrons, where n_s is the number of surface atoms (*viz.*, 12) and Δ_i is the electron count characteristic of the central atom or atom-fragment lying at the center of the cluster (*viz.*, 18 for one interior Pd atom). The overall electron count is then 204 electrons [*i.e.*, 162 + (3 × 48) (triangle) − (3 × 34) (edge)], which is in exact agreement with the observed electron count. The same electron count is obtained *via* the Teo/Zhang approach [39] for the condensation of a centered icosahedron with three common triangles through three bridging edges. A lower skeleton electron-pair *B* value of 9 (instead of 13) for the centered icosahedron in **1** gives rise to an overall cluster bonding *B* value of 12 [*i.e.*, 9 (icosahedron) + 3(6) (triangle) − 3(5) (edge)] for the entire Pd_{16} core. Based upon a close-packed high-nuclearity metal cluster, the overall calculated electron count in the Teo/Zhang model [39] is given by $2(6S_n + B)$. For **1** with $S_n = 15$ (*i.e.*, the total number of surface atoms) and $B = 12$, the resulting electron count is 204. This model, which likewise predicts the same lower (than normal) total electron count for **1**, is completely consistent with *tangential* palladium surface bonding interactions being negligible.

(b) $Pd_{35}(CO)_{23}(PMe_3)_{15}$ 2. The observed electron count for **2** is (35 × 10) (Pd) + (23 × 2) (CO) + (15 × 2) (PMe_3) = 426 electrons. The Mingos model [31] for the condensed pentaicosahedral Pd_{29} core gives $12n_s + \Delta_i = (12 \times 24) + 72 = 360$ electrons, where $n_s = 24$ surface atoms and $\Delta_i = 72$ for the $Pd(i)_5$ trigonal bipyramid (*i.e.*, because the trigonal bipyramid may be regarded as two tetrahedra sharing a common equatorial triangular face, the resulting electron count is (2 × 60) − 48 = 72). The capping of each of the three pseudo-C_3 related Pd(33), Pd(34) and Pd(35) atoms to a triangular face of the Pd_{29} fragment can be envisioned as a condensation of a tetrahedron to the core through a common triangular face; the condensation rule then gives rise to an additional electron count of 60 − 48 = 12 electrons. Each of the three pseudo-C_3 related Pd(27), Pd(28) and Pd(29) atoms caps the four atoms of two edge-common triangular faces of the Pd_{29} core; this corresponds to the condensation of the Pd_{29} core with a trigonal bipyramid (*viz.*, 72 electrons) through two edge-sharing "butterfly" triangles [*viz.*, (2 × 48) − 34 = 62 electrons], resulting in an additional electron count of 72 − 62 = 10 electrons. The overall predicted electron count would then be 360 + (3 × 12) + (3 × 10) = 426 electrons, which agrees exactly with the observed electron count.

(c) $Pd_{39}(CO)_{23}(PMe_3)_{16}$ 3. Due to irregular condensation-patterns of the 16 Pd atoms with one another and with the central face-fused Pd_{23} biicosahedron, there appears to be no appropriate electron-counting approach that can provide a reliable electron count.

(d) $Pd_{59}(CO)_{32}(PMe_3)_{21}$ 4. Each of the identical two halves of the 59-atom metal core consists of a centered icosahedron which is partially covered by a layer of 18 Pd atoms [with the exclusion of Pd(9) and its two threefold-related Pd(9A) and Pd(9B)]. Each half is composed of 31 atoms, of which four form an interior $Pd(i)_4$ tetrahedron [*viz.*, the icosahedral-centered Pd(5), and Pd(1) together with its two threefold-related Pd(1A), Pd(1F)]. Based on the Mingos model,[31] the electron count for each half is given by $12n_s + \Delta_i$, where $n_s = 27$ surface atoms and $\Delta_i = 60$ for a tetrahedron; the resulting electron count is 384 electrons. The two halves formally condense by the face-sharing of a common ν_2 Pd_6 triangle [*viz.*, (4 × 48) (triangle) − (3 × 34) (common edge) = 90 electrons]. The metal skeleton of **4** is completed by double-edge-sharing of the above 56-atom polyhedron with three square pyramids. The total predicted electron count for all of these condensations is (2 × 384) − 90 + (3 × 74) − 3 (2 × 34) = 696 electrons. This value is in exact agreement with the observed electron count of (59 × 10) (Pd) + (32 × 2) (CO) + (21 × 2) (PMe_3) = 696 electrons.

(e) $Pd_{29}Ni_3(CO)_{22}(PMe_3)_{13}$ 5. The observed electron count for **5** is (29 × 10) (Pd) + (3 × 10) (Ni) + (22 × 2) (CO) + (13 × 2) (PMe_3) = 390 electrons. The Mingos model [31] for the condensed tetraicosahedral Pd_{26} core (with a bonding interior $Pd(i)_4$ tetrahedron) gives $12n_s + \Delta_i = (12 \times 22) + 60 = 324$ electrons, where $n_s = 22$ surface atoms and $\Delta_i = 60$ for the $Pd(i)_4$ tetrahedron. The capping of each of the three equivalent Ni(4) atoms to a triangular face of the condensed tetraicosahedral Pd-core can be envisioned as a condensation of a tetrahedron with the core through a common triangular face; the condensation rule gives rise to an additional electron count of 60 − 48 = 12 electrons. Each of the three equivalent Pd(7) atoms caps the four atoms of two edge-common butterfly-like triangular faces of the condensed tetraicosahedral core, for which the electron count is (2 × 48) − 34 = 62 electrons. Because the electron count for a trigonal bipyramid is 72 electrons, the condensation of a trigonal bipyramid to the tetraicosahedral Pd_{26} core through two edge-common butterfly-like triangular faces results in the addition of 72 − 62 = 10 electrons to the electron count from each capping Pd(7). The resulting overall electron count would then be 324 + (3 × 12) (capping Ni) + (3 × 10) (capping Pd) = 390 electrons, which is in exact agreement with the observed electron count.

Comparative electron-counting analysis of 1–5 with centered Au, Au–Ag and Au–M (M = Pd, Pt) monoicosahedra and with vertex-sharing Au–Ag and Au–Ag–M (M = Ni, Pd, Pt) polyicosahedra, and resulting implications

The overall predicted electron count of 204 electrons obtained *via* the Mingos model [31] and the Teo/Zhang model [39] for the centered Pd_{13} icosahedron and three edge-bridged $Pd(PR_3)$ fragments in **1** is in exact agreement with the observed electron count (*viz.*, 204 electrons) only when a lower electron count of 162 electrons (Mingos model [31]) corresponding to a reduced skeletal electron-pair *B* value of 9 (Teo/Zhang model [39]) is utilized for the complete centered icosahedron per se (*i.e.*, the usual electron count is 170 electrons corresponding to $B = 13$).[32–38] Particularly noteworthy is that the same observed electron count of 162 electrons is observed in several complete centered monoicosahedra containing spherical coinage-metal cages: namely, the classic Au-centered Au_{12} cage in $[(\mu_{12}\text{-Au})(AuPMePh_2)_{10}(AuCl)_2]^{3+}$ ($[PF_6]^-$ salt),[40a] the Pd-centered Au_{12} cages in neutral $[(\mu_{12}\text{-Pd})(AuPPh_3)_8(AuCl)_4]$,[40b] and $[(\mu_{12}\text{-Pd})(AuPPh_3)_6(Au_2dppe)(AuCl)_4]$,[40c] the Au-centered Au_8Ag_4 cage in $[(\mu_{12}\text{-Au})(AuPMePh_2)_8(AgCl)_4]^+$ ($[C_2B_9H_{12}]^-$ salt),[40d] the Au-centered Au_8Ag_4 cage in the bromide $[(\mu_{12}\text{-Au})(AuPMePh_2)_8(AgBr)_4]^+$ analogue,[40e] and the Pt-centered Au_6Ag_6 cage, whose six Ag atoms are each connected to an iodide-bridging atom from two tridentate AgI_3 fragments, in neutral $[(\mu_{12}\text{-Pt})(AuPPh_3)_6(Ag(\mu_2\text{-I}))_6(\mu_3\text{-Ag})_2]$.[40f] Mingos [31b] stated that a lower electron-counting value for a high-nuclearity metal cluster would arise when *radial* interactions between the centered (interior) metal and surface metals predominate. In $[(\mu_{12}\text{-Au})(AuPMePh_2)_{10}(AuCl)_2]^{3+}$, the contributions of the pair of

tangential valence p AOs (*viz.*, p_x, p_y) per surface gold atom are thereby assumed to be negligible due to these two valence p AOs being energetically too high to participate in the surface bonding; this consequence has been attributed to relativistic effects being especially large for gold.[41] The dominant *radial* metal–metal bonding interactions between the valence s AOs of the surface gold atoms (*i.e.*, the valence p_z AOs are assumed under a localized bonding description to be involved with Au–ligand bonding), and the one valence s and three p AOs of the centered gold atom result in the formation of four strongly bonding MOs that are occupied by 8 skeletal electrons; the other 10 electrons of the 18-electron contribution of the centered gold atom in the Mingos model[31b] occupy the five valence d AOs which are presumed to be essentially nonbonding (or at most weakly bonding). Hence, the centered $5d^{10}6s^1$ Au atom in the Au_{13} icosahedron is considered to contribute only one valence electron to the skeletal electron-pair count. It is apparent that similar energetic arguments resulting in negligible tangential surface bonding interactions for the Pd-centered Pd_{12} icosahedral cage in **1** must be applied in order to account for the same lower observed electron-counting value, even though relativistic effects are much smaller in Pd than in Au.

Of relevance is an examination of electron-counting consequences resulting from the formation of polyicosahedral clusters. A remarkable series of *vertex-sharing polyicosahedral* Au–Ag and Au–Ag–M (M = Ni, Pd, Pt) clusters have been systematically prepared and investigated both experimentally and theoretically by Teo/Zhang and coworkers.[42] One of the initially characterized 25-atom $Au_{13}Ag_{12}$ clusters formed by two centered icosahedra sharing one vertex is the $[Au_{13}Ag_{12}\{P(p\text{-tol})_3\}_{10}Br_2(\mu_2\text{-Br})_2(\mu_3\text{-Br})_4]^+$ monocation ($[PF_6]^-$ salt),[43] which has a staggered–staggered–staggered (sss) rotameric configuration for its four metal pentagons with *two* doubly and *four* triply bridging bromide ligands coordinated to the 10 Ag atoms comprising the two inner pentagons;[43–46] Teo and Zhang[39] showed that its observed electron count of 322 electrons is in exact agreement with the calculated electron count obtained from their model, in which they utilized a normal *B* value of 13 per icosahedron. Noteworthy is that the same calculated electron count is obtained for this cluster *via* the Mingos condensation rule[31] if an electron count of 170 electrons is utilized for each icosahedron [*i.e.*, $(2 \times 170) - 18 = 322$]. However, for other vertex-sharing biicosahedra the *observed* electron counts are significantly smaller than 322 electrons: for example, $[Au_{13}Ag_{12}\{P(p\text{-tol})_3\}_{10}Cl_2(\mu_2\text{-Cl})_5]^{2+}$ ($[SbF_6]^-$ salt) (310 electrons) containing a nearly staggered–eclipsed–staggered (ses) rotameric metal configuration with *five* doubly bridging chloride ligands[47] and neutral $[Au_{12}Ag_{13}(PMePh_2)_{10}Br_2(\mu_2\text{-Br})_7]$ (318 electrons) containing a sss rotameric metal configuration with *seven* doubly bridging bromide ligands.[48] These dissimilar *observed* electron counts for known vertex-fused biicosahedral Au–Ag clusters are governed by the different number of bridging halide atoms and their particular modes of Ag-linkages along with the overall charge.

The one crystallographically analyzed vertex-sharing example of a 36-atom triicosahedral Au–Ag cluster consisting of three Au-centered icosahedra sharing three vertices (in a cyclic fashion) is neutral $[Au_{18}Ag_{20}(P(p\text{-tol})_3)_{12}Cl_2(\mu_2\text{-Cl})_6(\mu_3\text{-Cl})_6]$, for which the observed electron count is 492 [*i.e.*, $N_{obs} = (18 \times 11)$ (Au) + (20×11) (Ag) + (12×2) (PR_3) + (2×1) (Cl) + (6×3) (μ_2-Cl) + (6×5) (μ_3-Cl) = 492]. Because this cluster has two extra nonbonding exopolyhedral atoms,[49] Teo and Zhang[39] showed that (with their exclusion) the observed electron count for its vertex-sharing triicosahedral $Au_{18}Ag_{18}$ core of 456 electrons [*i.e.*, $492 - (2 \times 18) = 456$] is in exact agreement with their model, in which they again used a *B* value of 13 for each icosahedron [*i.e.*, $B = (3 \times 13)$ (icosahedron) $- (3 \times 3)$ (vertex) = 30; $N = 2T = 2(V_m + B) = 2[(6 \times 33) + 30] = 456$}. The same electron count is also calculated by use of the Mingos condensation rule[31a] when an electron count of 170 electrons per icosahedron is used [*i.e.*, (3×170) (icosahedron) $- (3 \times 18)$ (vertex) = 456].

Teo *et al.*[48] pointed out that all of the known 25-atom vertex-sharing Au–Ag biicosahedra have an overall cluster charge of +2 for *five* bridging halides, +1 for *six* bridging halides, and 0 for *seven* bridging halides, while for corresponding Au–Ag–M biicosahedra (M = Ni, Pd, Pt) containing only one M-centered icosahedron (*i.e.*, the other icosahedral center still being Au) the resulting overall positive charge is reduced by one.

Based upon a EHMO analysis of closed-shell electronic requirements for the Teo/Zhang polyicosahedral coinage-metal clusters with two and three icosahedral sharing vertices, Mingos and coworkers[50] stated that (unlike transition metal carbonyl clusters generally containing closed-packed metal arrangements) the usual cluster-bonding approaches involving the total number of valence cluster electrons are not applicable. Because their calculations also indicated that the *intericosahedral* metal–metal interactions for vertex-sharing icosahedra are relatively weak compared to *intraicosahedral* ones, they proposed that the closed-shell requirements for vertex-linked icosahedra are simply associated with the four strongly bonding filled radial skeletal MOs (or eight valence electrons) per icosahedron. Consequently, clusters with two and three icosahedra sharing vertices have 16 and 24 valence electrons, respectively, for radial skeletal metal–metal bonding. Furthermore, this scheme presumes that the radial skeletal metal–metal bonding primarily involves the valence *n*s coinage-metal AOs ($n = 5$, Ag; $n = 6$, Au) for the surface (cage) metal atoms and that the $(n - 1)$d metal valence electrons and metal–ligand bonds can be ignored even though radial surface metal valence np_z AOs are utilized (under a localized bonding scheme) for accepting electron pairs from ligand lone-pair orbitals.

This simple bonding scheme[50] is completely compatible with the observed electron counts in the known centered monoicosahedral and polyicosahedral coinage-metal clusters. However, it should be noted that the 162-electron count for the known complete centered monoicosahedral metal–coinage clusters (*vide supra*) corresponds to the eight valence-electron scheme for radial skeletal metal–metal bonding under the provision that 24 valence electrons are necessary for the bonding of the ligands to the 12 metal–coinage cage atoms.

Of prime interest is whether the 162-electron **1**, similarly reformulated as $[(\mu_{12}\text{-Pd})(PdPMe_3)_6(PdCO)_6\{\mu_2\text{-Pd}(CO)_2(PMe_3)\}_3(CO)]$, also conforms to the eight-electron valence count. The rewritten formula formally denotes the assignment of a two-electron donating phosphine or CO ligand to each of the 12 cage atoms. Each of the three 16-electron edge-bridging $\mu_2\text{-Pd}(CO)_2PMe_3$ exopolyhedral ligands, which has a trigonal-planar ligand array of one PMe_3 and two bridging COs, may be viewed as a two-electron donor to its two edge-bridged Pd atoms in the Pd_{12} cage (*i.e.*, for the edge-condensation of an exopolyhedral triangular metal fragment with a metal polyhedron, the formal electron count is 14 electrons corresponding to 48 electrons for a metal triangle minus 34 electrons for a common metal edge). The three edge-bridging $\mu_2\text{-Pd}(CO)_2PMe_3$ exopolyhedral ligands and the remaining CO may then be considered as formally furnishing the required number of eight valence electrons for radial skeletal metal–metal bonding.

One salient bonding feature that emerges from this detailed comparison is that the vertex-sharing biicosahedral $[Au_{13}Ag_{12}\{P(p\text{-tol})_3\}_{10}Br_2(\mu_2\text{-Br})_2(\mu_3\text{-Br})_4]^+$ monocation and vertex-sharing triicosahedral neutral $[Au_{18}Ag_{20}\{P(p\text{-tol})_3\}_{12}Cl_2(\mu_2\text{-Cl})_6(\mu_3\text{-Cl})_6]$ cluster conform not only to the electron-counting models of Mingos[31] and Teo/Zhang[39] but also to the eight valence-electron scheme[50] per icosahedron.

In light of the lower than normal icosahedral electron count observed in **1** and the dissimilar observed electron counts for different vertex-sharing 25-atom biicosahedra (*vide supra*), it is perhaps somewhat surprising that the observed electron counts

for the highly condensed icosahedral-based geometries of **2**, **4** and **5** agree exactly with the corresponding calculated electron counts based upon the Mingos rules[31] for face-condensed polyhedra. This electron-counting agreement provides strong evidence that the resulting composition and geometry of each of these complex palladium clusters are stabilized *via* electronic effects as well as *via* protective shielding of the metal core by the surrounding ligand arrangement.

The above similarities and differences and resulting electronic implications indicated by electron-counting rules for analogous clusters containing icosahedral centered palladium cages *versus* coinage-metal (Group 11) cages illustrate that electron-counting procedures are generally invaluable in successfully correlating the geometries of small-to-large transition metal clusters to their observed numbers of cluster valence electrons, and in the examples given above they provide illuminating insight concerning closed-shell electronic requirements for both vertex- and face-condensed transition metal/coinage metal clusters. However, these examples also illustrate that one must be extremely careful in their utilization in that electron-counting models do *not* necessarily provide an unambigous physical description concerning the actual nature of the electron-pair distributions in a transition metal cluster.[51a] This conclusion is completely consistent with the view stated by Woolley[51b] that the isolobal principle and electron-counting rules owe their generality and utility to being symmetry-based, but that the energetics and details of the electronic structures of transition metal clusters are a separate manner requiring appropriate methods of theoretical chemistry.

Synthesis and characterization

Reactions of phosphine ligands with metal carbonyl clusters generally result either in carbonyl substitution[10,52] or a series of degradation reactions[13,16] leading to products which do not bear any simple relationship to the starting compounds. The use of acid to create a specific equilibrium concentration of free phosphine which is optimal for the formation of the clusters with appropriate structures has been discussed.[9,10,53] Mednikov *et al.*[9–16] have obtained high-nuclearity palladium carbonyl phosphine clusters (*vide supra*) by use of phosphines as stabilizing ligands along with a carboxylic acid as a buffer in solution to control the free phosphine concentration which thereby allows the growth of large clusters; each of their remarkable clusters has either PEt_3 or PBu^n_3 ligands.

Our choice of trimethylphosphine as a reactant to form new trimethylphosphine-stabilized palladium carbonyl clusters was based upon the premise that less bulky trimethylphosphine ligands would likely play an important steric role in stabilizing clusters with still larger metal-core sizes. This goal was essentially achieved in that the geometrically unprecedented palladium cores of **2**, **3**, **4** and **5** are all unusually large; in fact, the initially reported nanosized Pd_{59} core in **4** held the world record[25] (until last year) in possessing the largest crystallographically determined transition-metal core with direct metal–metal bonding. This record was demolished with the recent advent of the nanosized $Pd_{145}(CO)_x(PEt_3)_{30}$.[18]

Highly reproducible reactions of a Pd–Ni carbonyl cluster **A** with PMe_3 (in the presence of acetic acid) afforded **1**, **2**, **3** and **4** in moderate yields of ≈16% for **1**, ≈15% for **2**, ≈27% for **3** and ≈40% for **4**. Reactions of **A** with PMe_3 (without acetic acid) produced a much larger yield (≈52%) for **1** as the major product along with **5** as a minor product (<5%). Different sets of reaction conditions were carried out in order to optimize the product yields. In addition to kinetic factors, adjusted variables that influenced cluster formation included the mole ratios and concentrations of the reactants, as well as the reaction time.

The compositions established by the CCD X-ray crystallographic determinations for the four homopalladium clusters (*viz.*, **1**, **2**, **3**, **4**) are in complete agreement with the elemental analyses. These four clusters were also characterized by IR, multinuclear NMR, and cyclic voltammetry; because the Pd–Ni species **5** was isolated in very low yields, both its molecular geometry and composition were determined from the X-ray diffraction analysis along with IR.

For both $Pd_{39}(CO)_{23}(PMe_3)_{16}$ **3** and $Pd_{59}(CO)_{32}(PMe_3)_{21}$ **4**, only a weighted average signal in the ^{31}P NMR spectra was observed at room temperature and at −60 °C. This effect may be a consequence of relatively low-energy dynamic exchange processes occurring in solution, whereby the chemically different phosphine ligands become equivalent at the coalescence temperature (< −60 °C). The fact that no detectable ^{13}C methyl resonances were observed in ^{13}C NMR spectra of $Pd_{35}(CO)_{23}(PMe_3)_{15}$ **2**, $Pd_{39}(CO)_{23}(PMe_3)_{16}$ **3** or $Pd_{59}(CO)_{32}(PMe_3)_{21}$ **4** may be attributed to peak broadening effects. CVs of each homopalladium cluster did not exhibit any reduction waves (out to −2.8 V) or oxidation waves (out to +1.0 V).

Stereochemical interrelationships

Of prime interest is that all of the five clusters exhibit icosahedral-based metal architectures. Centered icosahedra have been implicated as structural units in a wide variety of amorphous materials[54] and in the formation and growth of small metal particles.[55] A general survey of structure/bonding relationships of a wide variety of inorganic materials that have icosahedral structures is given by King.[56] A recent comprehensive review by Belin and coworkers[57] summarizes the structural features, bonding, and electronic requirements resulting from the widespread icosahedral oligomerization and condensation of intermetallics, especially for the Group 13 elements (B, Ga).

A large number of crystallographically determined high-nuclearity transition metal clusters have metal-core geometries formally derived from the condensation of tetrahedral, octahedral and trigonal prismatic units.[2] The metal-core geometries in **1**, **2**, **3**, **4** and **5** reported herein provide illuminating information regarding particular condensations of centered transition-metal icosahedral units with each other as well as with other transition-metal polyhedra.

Moreover, these clusters exhibit the following salient features:

(1) The face-condensed growth patterns resulting in the core-geometries in **2**, **3**, **4** and **5** presumably involve the initial formation of central icosahedral-based palladium fragments that undergo further face-condensations with other polyhedra as well as face-capping of atoms. Central fragments in **2** and **3** may arise from direct face-sharing of two palladium icosahedra, while in **4** the central Pd_{29} fragment of crystallographic D_3 symmetry is composed of two centered icosahedra that are indirectly connected by face-fusions with an inner palladium bioctahedron on its two opposite triangular faces.

In sharp contrast, the general growth sequence of the extraordinary centered polyicosahedral Au–Ag and Au–Ag–M supraclusters (M = Ni, Pd, Pt), prepared and experimentally/theoretically characterized by Teo, Zhang and coworkers,[42–49] was formulated as vertex-condensations of centered icosahedral building blocks. In addition to kinetic factors, it is apparent that the existence of ligated icosahedral-based metal clusters critically depends upon the cohesive energies of the metal atoms and combined electronic/steric effects of its ligands.

(2) Large clusters tend to have structures that minimize their surface energy by forming spheroidal-like metal polyhedra with certain geometric distortions, as found in the previously reported $Pd_{16}(CO)_{13}(PEt_3)_9$,[12] $Pd_{23}(CO)_{22}(PEt_3)_{10}$,[13] $Pd_{23}(CO)_{20}(PEt_3)_8$,[14] and $Pd_{38}(CO)_{28}(PEt_3)_{12}$.[15,16] Spheroidal-like metal polyhedra are also observed for $Pd_{16}(CO)_{13}(PMe_3)_9$ **1**, $Pd_{35}(CO)_{23}(PMe_3)_{15}$ **2**, $Pd_{39}(CO)_{23}(PMe_3)_{16}$ **3** and $Pd_{29}Ni_3(CO)_{22}(PMe_3)_{13}$ **5**. However, $Pd_{59}(CO)_{32}(PMe_3)_{21}$ **4** displays an ellipsoidal-like metal polyhedron due to its elongated central Pd_{29} fragment.

(3) Both **2** and **3** contain a 23-atom face-fused biicosahedron (also denoted as a twinned icosahedron). This direct face-sharing condensation of either two non-centered or two centered icosahedra is unprecedented for transition metal clusters. There are a few examples of face-sharing between two *non-centered* icosahedra possessing Group 13 main-group elements (B, Ga). Discrete molecular compounds having an analogous non-centered polyhedral condensation are $B_{20}H_{16}(NCMe)_2$,[58] which possesses a direct triangular face-sharing of a B_{12} icosahedron with a B_{11} icosahedral fragment, and $[(Pt_2\text{-}\eta^4,\eta^6\text{-}anti\text{-}B_{18}H_{16})(PMe_2Ph)_4]$,[59] in which a *nido*-platinaundecaborane and a *closo*-platinadodecaborane are face-fused *via* a common triangular B_3 face. In addition, X-ray crystallographic analyses have uncovered face-fused *non-centered* icosahedral M_{21} dimers (also referred to as twinned icosahedra) in solid-state intermetallic phases of gallium and boron.[57] The only non-defective example is the *twinned* B_{21} icosahedral fragment present in β-tetragonal boron;[60a] atom-defective twinned non-centered icosahedral fragments are observed in several gallium intermetallics including $Li_9K_3Ga_{28.83}$,[60b] $Li_3Na_5Ga_{19.56}$,[60c] and $Na_{6.25}Rb_{0.60}Ga_{20.02}$.[60d] In each of these solid-state structures 18 of the 21 icosahedral atoms (*i.e.*, other than the face-shared triangular atoms) are *exo*-linked to neighboring icosahedra. Extended Hückel calculations by Burdett and Canadell and by King[61–63] and by Belin and coworkers[57] of model $Ga_{21}H_{14}$ and $M_{21}H_{18}$ species (M = B, Ga), in which hydrogen ligands were used to simulate *exo* bonds, revealed a marked stabilization of atom-defective polyhedra in which antibonding interactions between neighboring intericosahedral atoms are suppressed. It was pointed out that the stabilization of these solid-state twinned icosahedra may also depend upon packing limitations, polarization and size-tuning with alkali metal cations.

(4) The ligand-to-metal (L/M) ratio is observed to decrease significantly with an increase in size of the icosahedral-based metal core for these five icosahedral-based Pd and Pd–Ni carbonyl phosphine clusters: namely, 22/16 = 1.38 in **1**, 35/32 = 1.09 in **5**, 38/35 = 1.09 in **2**, 39/39 = 1.00 in **3** and 53/59 = 0.90 in **4**. Despite the large variation in cluster cone angle between the relative bulky trimethylphosphine and carbonyl ligands, this trend in L/M ratios roughly reflects fewer ligands per metal atom with an increased number of face-condensed metal atoms. The ligand-to-surface metal ratio of 22/15 = 1.47 in **1**, 35/28 = 1.25 in **5**, 38/30 = 1.27 in **2**, 39/34 = 1.15 in **3** and 53/48 = 1.10 in **4** shows the same trend of fewer ligands per surface metal atom for the larger metal cores in this cluster series. This variation may be attributed to interligand steric constraints coupled with an inverse correlation in a ligated metal cluster between the number of metal connectivities to a given metal atom and the number of bound ligands. Particularly noteworthy is that for these five metal clusters the number of completely encapsulated interior metals also increases with the increased size of the metal core; namely, one in **1**, four in **5**, five in **2** and **3**, and 11 in **4**.

A similar observed trend involving a decrease in the maximum number of COs per surface metal atom with an increase in size of the metal-core polyhedron in large metal carbonyl clusters was initially pointed out by Chini[1] who also stated that the existence of unusually large carbonyl clusters for the late transition metals is probably due to the decreased number of carbonyls required on electronic grounds.

(5) In these large phosphine-stabilized palladium carbonyl clusters, the tertiary phosphine ligands shield the surfaces of the metallic frameworks much better than carbonyl ligands and thus offer more efficient steric stabilization of the cluster.[64] However, the bulkiness and number of PR_3 ligands as well as the number of bridging CO ligands must be in an allowable proportion to reach a high ligand-stabilized efficiency. For example, $Pd_{16}(CO)_{13}(PMe_3)_9$ **1**, $Pd_{35}(CO)_{23}(PMe_3)_{15}$ **2**, $Pd_{39}(CO)_{23}(PMe_3)_{16}$ **3**, $Pd_{59}(CO)_{32}(PMe_3)_{21}$ **4** and $Pd_{29}Ni_3(CO)_{22}(PMe_3)_{13}$ **5** possessing sterically less demanding PMe_3 ligands (*i.e.*, smaller cone angle) have higher ratios of PR_3/CO ligands (from 0.59 to 0.69) compared to those of 0.45, 0.40 and 0.43 in $Pd_{23}(CO)_{22}(PEt_3)_{10}$,[13] $Pd_{23}(CO)_{20}(PEt_3)_8$,[14] and $Pd_{38}(CO)_{28}(PEt_3)_{12}$,[15,16] respectively.

(6) A comparison of mean Pd(i)–Pd(i), Pd(i)–Pd(s) and Pd(s)–Pd(s) connectivities in each of these clusters shows that upon an increase in palladium nuclearity (which normally coincides with an increase in the number of interstitial atoms), the mean connectivities for the above mentioned three types of bonding Pd–Pd distances approach one another and are closer to the Pd–Pd distance (2.75 Å) in ccp palladium bulk metal,[30] even though large variations in the Pd–Pd distances are observed for each type.

Envisioned growth pathways in the self-generation of the highly condensed icosahedral-based metal cores of 2, 3, 4 and 5

The atom-by-atom growth pattern of partial icosahedral fragments resulting in the complete 13-atom centered icosahedron (such as in **1**) is well-documented.[42d,65] This growth process is based upon a maximization of nearest-neighbor contacts. By use of a "clusters-of-clusters" growth concept, Teo and Zhang[42c,d] have analyzed their particular series of coinage-metal polyicosahedral clusters in terms of a well-defined vertex-sharing growth pathway in which the basic building block is the 13-atom centered icosahedron. Teo, Zhang and co-workers[42e] have also performed calculations of metallic energies and relative energies of binary icosahedral clusters.

Although the icosahedral-based palladium core geometries of **2**, **3**, **4** and **5** differ greatly from one another, their indicated electronic closed-shell stabilities, evidenced from the exact agreement between their observed and calculated electron counts, suggest that there is a general interrelated commonality in their growth patterns. We propose that the formation of each of these clusters involves the prior assembly of a certain icosahedral-based central palladium-core fragment by an organized synthetic route, which is concomitantly stabilized by face-condensations with additional carbonyl-ligated palladium atoms in order to conform to electronic/steric constraints. The fact that palladium metal has the lowest cohesive energy (*i.e.*, the weakest metal–metal bonding) of the Group 8–10 transition metals is presumed to be responsible for its unique tendency among the Group 8–10 metals to form highly-condensed icosahedral-like core-fragments.

A general growth sequence can be proposed that gives the *four* interpenetrating centered icosahedra comprising the pseudo-T_d Pd_{26} central part of the $Pd_{29}Ni_3$ core in **5** and the *five* interpenetrating centered icosahedra comprising the pseudo-D_{3h} Pd_{29} central part of the Pd_{35} core in **2**. This growth process (Fig. 6), which also is based upon the maximization of nearest-neighbor connectivities, involves the addition of atoms onto each adjacent face surrounding a given vertex of a centered icosahedron to give a new pentagonal pyramid. If the centered icosahedron is viewed as a cyclic face-condensation of 20 identical (but slightly deformed) tetrahedra that have a common vertex (*i.e.*, the centered atom) and share three faces with adjacent tetrahedra,[27,28] each atom addition may be considered as the face-fusion of two tetrahedra. This formal face-condensation construct would produce interpenetrating icosahedra: first, a D_{5h} Pd_{19} core consisting of *two* interpenetrating icosahedra (as yet unknown) and then a D_{3h} Pd_{23} core consisting of *three* interpenetrating icosahedra (also unknown). Further face-condensations would result in a T_d Pd_{26} core that corresponds to the central part of the $Pd_{29}Ni_3$ core in **5** followed by a D_{3h} Pd_{29} core that corresponds to the central part of the Pd_{35} core in **2**. This resulting growth pattern (depicted in Fig. 6) of interpenetrating centered icosahedra with the centred atoms forming strongly bonding interior kernels may be readily visualized in Fig. 7, in which each 13-atom centred icosahedron is represented as a sphere.

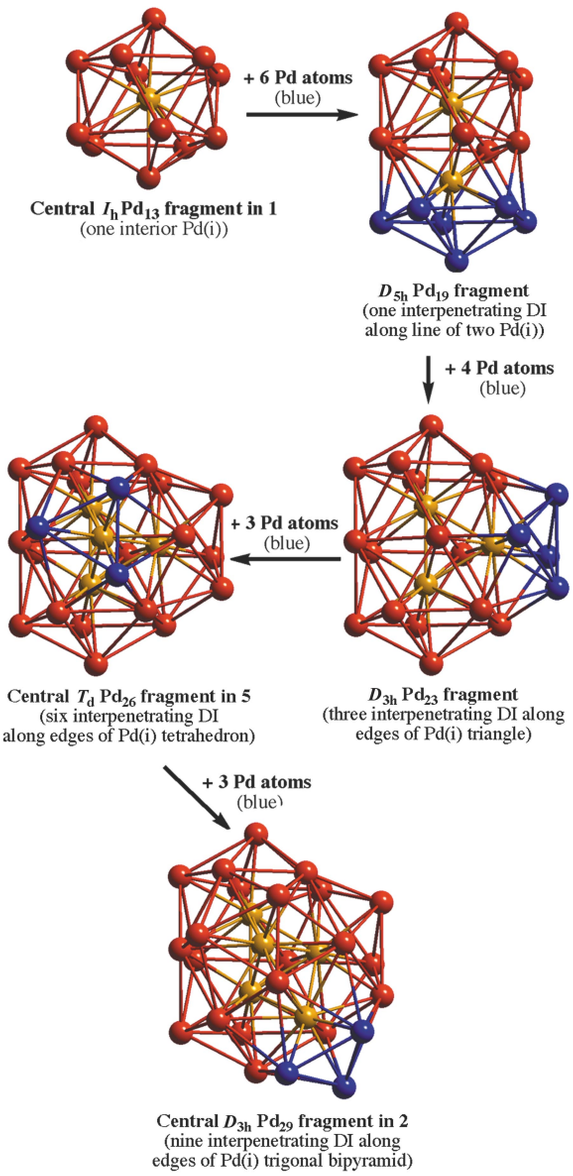

Fig. 6 Proposed atom-by-atom growth sequence from the centered Pd_{13} icosahedral fragment in $Pd_{16}(CO)_{13}(PMe_3)_9$ **1** generating the 26-atom central fragment in $Pd_{29}Ni_3(CO)_{22}(PMe_3)_{13}$ **5** and the 29-atom central fragment in $Pd_{35}(CO)_{23}(PMe_3)_{15}$ **2**. The central Pd_{26} fragment in **5** consists of *four interpenetrating* centered icosahedra forming *six* double icosahedral (DI) units along the six bonding edges of the centered $Pd(i)_4$ tetrahedron (gold); the central Pd_{29} fragment in **2** possesses *five interpenetrating* centered icosahedra forming *nine* double icosahedral (DI) units along the nine bonding edges of the centered $Pd(i)_5$ trigonal bipyramid. There are no reported examples of the presumed intermediate 19-atom double icosahedral (DI) and 23-atom triicosahedral fragments.

Our proposed cluster-growth pattern of **5** and **2** is analogous to the previously constructed interpenetrating icosahedral models described by Farges *et al.*[66] to account for particularly strong peaks (with the magic-number sequence of 13, 19, 23, 26, 29, 32 and 34) in the mass spectrum of charged gaseous argon clusters formed in a free-jet expansion into a vacuum.[67] Their constructed models[66] composed of double icosahedral (DI) units, consist of 19 atoms (two interpenetrating icosahedra forming two DI), 23 atoms (three interpenetrating icosahedra forming three DI), 26 atoms (four interpenetrating icosahedra forming six DI), 29 atoms (five interpenetrating icosahedra forming nine DI), *etc*. The pseudo-T_d central 26-atom polyhedron of the face-condensed $Pd_{29}Ni_3$ core in **5** and the pseudo-D_{3h} central 29-atom polyhedron of the face-condensed

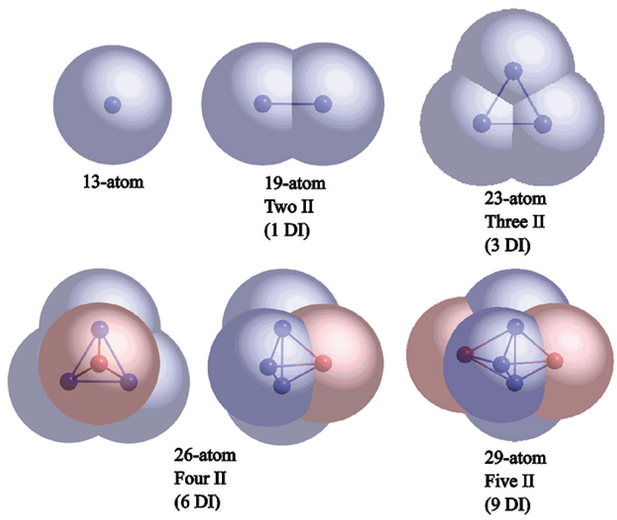

Fig. 7 Conceptual view of the growth pattern of interpenetrating icosahedra (II) forming double icosahedra (DI) involving maximization of nearest neighbor connectivities.

Pd_{35} core in **2** represent the first crystallographic examples of *four* interpenetrating centered icosahedra and *five* interpenetrating centered icosahedra, respectively.

The similarity of our proposed interpenetrating icosahedral growth pattern of the central palladium-core fragment in **5** and **2** from a centered icosahedral Pd_{13} fragment in **1** with the analogous growth pattern previously postulated by Farges *et al.*[66] for obtaining corresponding particularly stable, large argon clusters formed about positive ions in a free jet expansion[67] provides compelling evidence that the nature of the delocalized Pd–Pd bonding in these ligated palladium clusters may be described primarily in terms of attractive dispersion forces. One can thereby regard palladium (which has an atomic $4d^{10}$ closed-subshell ground state) as the only known Group 8–10 transition metal that can simulate an argon atom in forming analogous icosahedral-based clusters, which in the case of palladium can be stabilized by appropriate CO or phosphine ligands.

Another distinctly different mode of icosahedral-based cluster-growth (Fig. 8) involves a prior face-condensed twinning of two centered icosahedra to give the central Pd_{23} face-sharing biicosahedron found in both **2** and **3**. However, in **3** the asymmetric face-condensations with the 16 other capping Pd(c) atoms produce a large pseudo-C_{2v} bending deformation of the Pd_{23} fragment, whereas in **2** the face-fused Pd_{23} icosahedral fragment preserves its pseudo-D_{3h} symmetry upon further face-condensations of six of the 12 additional Pd atoms, resulting in the highly condensed central interpenetrating Pd_{29} pentaicosahedral fragment. Although this central Pd_{29} fragment in **2** can thereby be formed from both proposed pathways, particularly noteworthy is that the central Pd_{26} fragment (consisting of four interpenetrating icosahedra) in **5** cannot be formally constructed *via* this latter cluster-growth pathway. A third type of icosahedral-based cluster-growth pattern illustrated by **4** involves the prior formation of a central fragment by the face-sharing of a centered icosahedron with an octahedral polyhedron; in **4** the central Pd_{29} fragment is formed by the face-sharing of each of the two opposite triangular faces of a bioctahedron with an icosahedron.

Experimental

General comments on materials and techniques

All reactions and manipulations were carried out under an atmosphere of dry nitrogen *via* standard Schlenk techniques

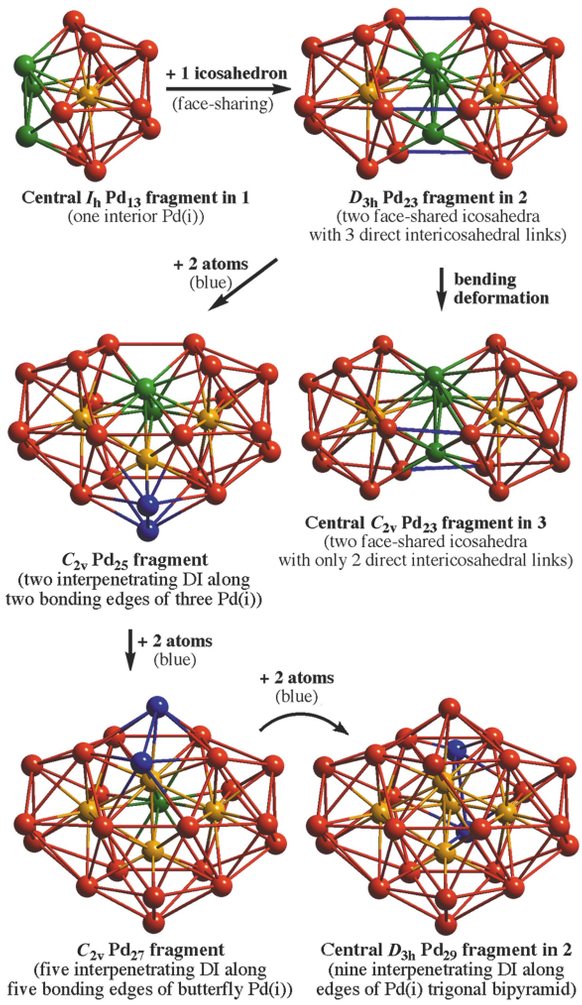

Fig. 8 Another proposed growth sequence from the centered Pd_{13} icosahedral fragment in $Pd_{16}(CO)_{13}(PMe_3)_9$ **1** generating the 23-atom central fragment in $Pd_{39}(CO)_{23}(PMe_3)_{16}$ **3** and the 29-atom central fragment in $Pd_{35}(CO)_{23}(PMe_3)_{15}$ **2**. The pseudo-D_{3h} Pd_{23} fragment (found in **2**) containing two icosahedra connected by a common face-sharing Pd_3 triangle (green) with *three* additional direct intericosahedral links is presumed to be initially formed; subsequent formation of the pseudo-C_{2v} central Pd_{23} fragment in **2** with only *two* direct intericosahedral links formally arises from a large bending deformation of the two face-sharing icosahedra from each other by ≈15° such that only one of the three intericosahedral links is broken. Face-condensation of the pseudo-D_{3h} Pd_{23} fragment by three successive pairs of connected Pd atoms (blue) produces the pseudo-D_{3h} central Pd_{29} fragment in **2** *via* a pathway containing the unknown pseudo-C_{2v} Pd_{25} and Pd_{27} intermediates.

or within a Vacuum Atmospheres drybox. All solvents were dried and distilled under nitrogen immediately prior to use. The following drying agents were used: THF (K/benzophenone), diisopropyl ether (K/benzophenone), acetone ($CaCO_3$), MeOH (Mg) and acetonitrile (Na_2CO_3 or $CaSO_4$). DMSO, DMF and distilled water were thoroughly purged with nitrogen before use.

$[Me_4N]_2[Ni_6(CO)_{12}]$ was prepared by a modification of the general method of ref. 68. Other chemicals were purchased from Strem and used without further purification.

The crystal structures were determined from X-ray data collected with a SMART CCD area detector diffractometry system from a standard Mo sealed-tube generator. All NMR spectra were recorded on a Bruker AM-500 spectrometer. All NMR samples were prepared *via* a freeze–pump–thaw technique. All ^{31}P NMR spectra were reported with phosphoric acid as an external reference. Infrared spectra were recorded on a Nicolet 740 FT-IR spectrophotometer with nitrogen-purged CaF_2 cells.

Syntheses of $Pd_{16}(CO)_{13}(PMe_3)_9$ 1, $Pd_{35}(CO)_{23}(PMe_3)_{15}$ 2, $Pd_{39}(CO)_{23}(PMe_3)_{16}$ 3 and $Pd_{59}(CO)_{32}(PMe_3)_{21}$ 4 and bimetallic cluster $Pd_{29}Ni_3(CO)_{22}(PMe_3)_{13}$ 5

(a) Preparation and stereochemical characterization of the bimetallic Pd–Ni carbonyl cluster A. This cluster is the precursor used in obtaining **1**, **2**, **3**, **4** and **5**. In a typical reaction, $Pd(OAc)_2$ (0.40 g, 1.80 mmol) dissolved in 15 mL of DMSO was added dropwise over 20 min *via* a stainless steel cannula to a stirred solution of $[Me_4N]_2[Ni_6(CO)_{12}]$ (0.75 g, 0.90 mmol) in 30 mL of DMSO containing two pellets of NaOH (≈0.2 g) (*i.e.*, NaOH is not soluble in DMSO solution). The solution quickly changed from cherry red to a dark brown color. After 5 h NaOH pellets were removed by the transfer of the solution to another flask, after which a solution of Ph_4PBr (7.5 g) in 20 mL of MeOH was added. The slow addition of distilled, degassed water to the ice-cooled solution resulted in a dark brown precipitate which was filtered off and washed several times with degassed water, methanol and then exclusively with THF. A subsequent acetone extract from the solid gave 0.60 g of **A** (which is extremely air-sensitive and readily loses CO). An IR spectrum (in MeCN) exhibited carbonyl bands at 1874s and 2010s cm^{-1}.

The initial preparation and isolation of cluster **A** was an outgrowth of reactions designed by Bacon[24a] to obtain Pd–Ni carbonyl clusters, which at that time were non-existent. Although Bacon[24a] occasionally isolated small quantities of crystalline products, the crystals invariably were too small and/or weakly diffracting to even obtain lattice parameters with a standard scintillation point-detector diffractometer. Fortunately, a new-generation SMART CCD area-detector diffractometer (for use with Mo-Kα radiation) became available at that time. Bacon's subsequent X-ray examination of a few crystals, obtained from a room-temperature reaction of $Pd(OAc)_2$ with $[NMe_4]_2[Ni_6(CO)_{12}]$ in DMSO, resulted in diffraction data being acquired from only one crystal.[24] Although the structural determination was greatly hampered by extensive crystal decay during room-temperature data collection (*i.e.*, a low-temperature setup was not then available), the crystallographic analysis unambiguously revealed the existence of a 30-atom ccp metal-core geometry, even though the metal-core composition could not be definitively established due to the resulting poor quality of the X-ray data set. This unprecedented structure can be readily visualized as an edge-truncated 35-atom ν_4 tetrahedron (where ν_n designates $n + 1 = 5$ atoms along each of the six edges), which is minus five atoms along one edge that is perpendicular to the opposite remaining five-atom tetrahedral edge.

Elemental analysis data (Desert Analytics, Tucson, AZ) for cluster **A** gave observed elemental Pd : Ni : P mass ratios of 15.0 : 6.3 : 1.0 (or Pd : Ni : P mole ratios of 4.4 : 3.3 : 1.0) that closely correspond to the tentative formulation of $[PPh_4]_4[Pd_{30-x}Ni_x(CO)_y]$ ($x \approx 13$).[24a] Furthermore, this formulation is entirely consistent with the unit-cell size of the partially determined crystal structure.[24b] This 30-atom metal core of cluster **A** may also be described as a five-layer ccp triangular stacking arrangement. Its top four layers are stacked in a ccp [*a*(M) *b*(M_3) *c*(M_6) *a*(M_{10})] sequence. The overall polyhedral geometry of this 20-atom four-layer ν_3 metal framework is analogous to the pseudo-$T_d(\bar{4}3m)$ cubic geometry of the metal core found in the $[Pd_{16}Ni_4(CO)_{22}(PPh_3)_4]^{2-}$ dianion[69] and the $[Os_{20}(CO)_{40}]^{2-}$ dianion.[70] The fifth (bottom) 10-atom triangular M_{10} layer in cluster **A** forms a ccp linkage with the fourth triangular M_{10} layer, but its central atom is necessarily displaced by a translational shift from the perpendicular threefold axis that passes through the top four layers including the central interior atom in the fourth M_{10} layer; the pseudo-T_d symmetry of the top four layers is thereby reduced to one mirror plane (C_s) that contains the one five-atom edge in cluster **A**.

Particularly noteworthy is that the triangular pseudo-T_d

stacking arrangement of the 20 atoms in the top four layers of the 30-atom metal core of the cluster **A** tetraanion is also analogous to that determined for the top four layers in the 26-atom $Pd_{13}Ni_{13}$ core of the pseudo-C_{3v} (3*m*) $[Pd_{13}Ni_{13}(CO)_{34}]^{4-}$ tetraanion.[71] The only major geometrical difference between their metal-core architectures is that the bottom (fifth) six-atom triangular Ni_6 layer in the $Pd_{13}Ni_{13}$ cluster is formally replaced by the bottom (fifth) 10-atom triangular M_{10} layer in cluster **A**. The one interior metal atom in the fourth layer has a ccp metal environment in cluster **A** *cf.* a hcp metal environment in the $Pd_{13}Ni_{13}$ cluster.

The analogous solubility characteristics of both compounds are consistent with the two tetraanions having the same negative charge, and furthermore their similarity in metal-core architectures (except for the bottom layer) points to closely related growth patterns in solution. Subsequent attempts to isolate and crystallize cluster **A** have been (as yet) unsuccessful.

(b) Synthesis of 1–4 from reactions of A and PMe_3 under acidic conditions. Reaction of **A** with PMe_3 in acidic medium was initially performed in an attempt to obtain a PMe_3-substituted derivative of **A** for X-ray diffraction analysis.[24] However, complex reactions undoubtedly occur to give isolable **1**, **2**, **3** and **4**. In a typical reaction, 10 mL of deoxygenated acetic acid was added to 0.60 g of **A** in 30 mL of MeCN, after which 250 μL of PMe_3 dissolved in 10 mL of acetonitrile was added dropwise to the mixture. The reaction was stirred at room temperature for three days. The resulting precipitate was separated and washed with MeCN. Extraction with THF (2 × 5 mL) gave 0.05 g of a dark brown compound characterized as $Pd_{35}(CO)_{23}(PMe_3)_{15}$ **2**. No residue remained after this extraction. The filtrate from the reaction was dried *in vacuo* to give a dark brown solid, which was extracted initially with MeOH (4 × 15 mL), and then with THF (2 × 5 mL). This THF extract gave 0.05 g of a dark brown compound characterized as $Pd_{16}(CO)_{13}(PMe_3)_9$ **1**. The MeOH extract was dried under N_2 flow and washed with degassed water, and the resulting solid was then extracted first with diisopropyl ether (4 × 15 mL) and then with THF (2 × 5 mL). $Pd_{59}(CO)_{32}(PMe_3)_{21}$ **4** (0.11 g) and $Pd_{39}(CO)_{23}(PMe_3)_{16}$ **3** (0.08 g) were obtained from the diisopropyl ether and THF extracts, respectively. Average yields based on $Pd(OAc)_2$ are 16% for **1**, 15% for **2**, 27% for **3** and 40% for **4**.

(c) Synthesis of 1 and 5 from A and PMe_3 in the absence of acetic acid. In a typical reaction, a solution of 300 μL of PMe_3 in 5 mL of MeCN was added dropwise over 15 min to a stirred solution of 0.60 g of **A** in 20 mL of MeCN. An orange powder appeared immediately followed by some black crystals that appeared gradually. The reaction was kept at room temperature for three days. The precipitate was separated and washed with 2 × 20 mL of MeCN. The THF extract (2 × 5 mL) from the precipitate gave 0.16 g of the black cluster, **1**, with an estimated yield of ≈52% based on $Pd(OAc)_2$. The orange powder residue that remained was not characterized.

The filtrate from the reaction was dried under a N_2 flow. The resulting dark brown solid was then extracted with MeOH (4 × 15 mL) and THF (2 × 5 mL). A minor product, identified as $Pd_{29}Ni_3(CO)_{22}(PMe_3)_{13}$ **5**, formed a few crystals from a layering of the THF extract with diisopropyl ether and hexane. Attempts to characterize the other products were unsuccessful.

(d) Synthesis of 3 from A and PMe_3 in the presence of a small quantity of acetic acid. A mixture of 250 μL of acetic acid with 280 μL of PMe_3 in 15 mL of MeCN was added dropwise into a stirred solution of 0.60 g of **A** in 30 mL of MeCN. A black precipitate gradually appeared. The reaction was stirred for three days. The resulting black precipitate was filtered off and washed with 5 × 15 mL of MeCN and characterized as $Pd_{39}(CO)_{23}(PMe_3)_{16}$ **3**, with an estimated yield of 0.14 g (50%) based on $Pd(OAc)_2$.

X-Ray diffraction analyses for 1–5

(a) $Pd_{16}(CO)_{13}(PMe_3)_9$ 1. Cluster **1** was crystallized either by the slow diffusion of MeOH and H_2O over a concentrated DMSO solution of **1** at room temperature or by the layering of diisopropyl ether on top of a THF solution of **1**. A black plate-shaped crystal of dimensions 0.30 × 0.30 × 0.15 mm, obtained from the first method, was selected for structural analysis.

$[Pd_{16}(CO)_{13}(PMe_3)_9]\cdot 2MeOH\cdot 3H_2O$: trigonal, space group $P31c$, $a = b = 15.6242(2)$, $c = 20.2437(5)$ Å, $\alpha = \beta = 90$, $\gamma = 120°$, $V = 4{,}279.73(13)$ Å^3, $Z = 2$, $D_C = 2.227$ Mg m^{-3}. A sphere of 8757 data was collected with Mo-Kα radiation at 133(2) K *via* 0.3 ω scans over a 2θ range 3.62–51.88°; an empirical absorption correction was applied. Structural determination was obtained by direct methods. Anisotropic least-squares refinement (270 parameters/86 restraints) on 3240 independent merged reflections ($R_{int} = 0.054$) converged at $wR_2(F^2) = 0.086$ for all data; $R_1(F) = 0.032$ for 3189 observed data [$I > 2\sigma(I)$]. A solvated water and methanol molecule were disordered in one solvent region. The refined occupancy of methanol was 0.67(2), while that of water was [1 − 0.67(2)] = 0.33(2).

(b) $Pd_{35}(CO)_{23}(PMe_3)_{15}$ 2. Crystals of **2** were obtained from the layering of diisopropyl ether and hexane over a concentrated THF solution of **2**. A black plate-shaped crystal of dimensions 0.10 × 0.08 × 0.02 mm was selected for data collection.

$[Pd_{35}(CO)_{23}(PMe_3)_{15}]$: triclinic, space group $P\bar{1}$, $a = 16.6290(2)$, $b = 17.5060(2)$, $c = 25.0118(3)$ Å, $\alpha = 75.353(2)$, $\beta = 89.019(2)$, $\gamma = 83.392(2)°$, $V = 6997.16(14)$ Å^3, $Z = 2$, $D_C = 2.615$ Mg m^{-3}. A sphere of 45 307 data was collected with Mo-Kα radiation at 133(2) K *via* 0.3 ω scans over a 2θ range 2.46–50.00°; an empirical absorption correction was applied. Structural determination was obtained by direct methods. Anisotropic least-squares refinement (1270 parameters/684 restraints) on 23 072 independent merged reflections ($R_{int} = 0.137$) converged at $wR_2(F^2) = 0.287$ for all data; $R_1(F) = 0.101$ for 9948 observed data [$I > 2\sigma(I)$]. Restraints were applied to the displacement parameters of most of the light atoms.

(c) $Pd_{39}(CO)_{23}(PMe_3)_{16}$ 3. This compound forms black prismatic crystals obtained from the layering of diisopropyl ether on top of an acetone solution of **3**. A black prism-shaped crystal of dimensions 0.20 × 0.10 × 0.06 mm was glued with epoxy inside a 0.5 mm glass capillary for structural analysis.

$[Pd_{39}(CO)_{23}(PMe_3)_{16}]$: monoclinic, space group $C2/c$, $a = 41.372(7)$, $b = 16.132(4)$, $c = 33.060(5)$ Å, $\beta = 128.381(10)°$, $V = 17{,}296(6)$ Å^3, $Z = 4$, $D_C = 2.308$ Mg m^{-3}. A sphere of 29 463 data was collected with Mo-Kα radiation at 297(2) K *via* 0.3 ω scans over a 2θ range 3.58–46.58°; an empirical absorption correction was applied. Structural determination was obtained by direct methods. Anisotropic least-squares refinement (705 parameters/377 restraints) on 11 877 independent merged reflections ($R_{int} = 0.144$) converged at $wR_2(F^2) = 0.278$ for all data; $R_1(F) = 0.116$ for 6522 observed data [$I > 2\sigma(I)$]. Restraints were applied to the atomic displacement ellipsoids of most of the light atoms.

(d) $Pd_{59}(CO)_{32}(PMe_3)_{21}$ 4. Crystals of **4** were grown by the layering of hexane over an acetone–diisopropyl ether solution of **4**. A black needle-shaped crystal of dimensions 0.40 × 0.10 × 0.10 mm was selected for data collection.

$[Pd_{59}(CO)_{32}(PMe_3)_{21}]\cdot 3Me_2CO\cdot 1.5(Pri_2O)$: trigonal, space group $P\bar{3}12/c$, $a = b = 22.7815(3)$, $c = 28.0363(4)$ Å, $\gamma = 120°$, $V = 12601.3(3)$ Å^3, $Z = 2$, $D_C = 2.398$ Mg m^{-3}. A sphere of 26 966 data was collected at 133(2) K *via* 0.3 ω scans over a 2θ range 4.12–50.00°; an empirical absorption correction

applied ($\mu = 6.923$ mm^{-1} for Mo-Kα radiation). Structural determination was obtained by direct methods. Anisotropic least-squares refinement (409 parameters/142 restraints) on 7135 independent merged reflections ($R_{int} = 0.099$) converged at $wR_2(F^2) = 0.146$ for all data; $R_1(F) = 0.055$ for 4120 observed data [$I > 2\sigma(I)$]. The highest small residual peak obtained in the asymmetric part of the original final Fourier difference map was modeled on the basis of Pd–Pd distances as a Pd(13) atom in a subsequent least-squares refinement. The existence of Pd(13) in a unit cell necessitates (from physically impossible short distances) that a nearby carbonyl ligand, C(6)–O(6), be absent in the same unit cell; an occupancy factor a was assigned to Pd(13), and an occupancy factor $(1 - \alpha)$ to each of the C(6) and O(6) atoms. This refinement gave $a = 0.043(4)$ for Pd(13) and $(1 - \alpha) = 0.957(4)$ for the CO ligand in the crystal-averaged unit cell. If it is assumed that the additional independent Pd(13) atom also conforms to crystallographic D_3 (32) site symmetry, the resulting formula for the superimposed co-crystallized cluster would be $Pd_{65}(CO)_{26+x}(PMe_3)_{21}$. The x CO ligands that would be attached to Pd(13) and the five symmetry-related Pd atoms were expectedly not detected on a final difference map on account of the much lower scattering powers of the C and O atoms. Because this presumed Pd_{65} cluster occupies only 4% of the unit cells in the crystal structure of **4**, it is viewed as a small impurity that can be neglected. Restraints were placed only on the positional and displacement parameters of the crystal-disordered acetone and diisopropyl ether solvated molecules and of the independent PMe_3 group that lies on a crystallographic two-fold rotation axis.

(e) $Pd_{29}Ni_3(CO)_{22}(PMe_3)_{13}$ 5. This $Pd_{29}Ni_3(CO)_{22}(PMe_3)_{13}$ cluster **5** was obtained as a minor product from the reaction of the Pd–Ni cluster **A** with PMe_3 in the absence of the acetic acid buffer. A black prism-shaped crystal of dimensions 0.40 × 0.20 × 0.10 mm was selected for X-ray data collection.

$Pd_{29}Ni_3(CO)_{22}(PMe_3)_{13}\cdot 0.3C_4H_8O$: trigonal, space group $R3$, $a = b = 16.4877(2)$, $c = 38.2484(4)$ Å, $\alpha = \beta = 90$, $\gamma = 120°$, $V = 9{,}004.59(18)$ Å^3, $Z = 3$, $D_C = 2.704$ Mg m^{-3}. A sphere of 10 756 data was collected with Mo-Kα radiation at 133(2) K *via* 0.3 ω scans over a 2θ range 3.56–52.08°; an empirical absorption correction was applied. Structural determination was obtained by direct methods. Anisotropic least-squares refinement (434 parameters/441 restraints for the solvated THF molecules) on 6122 independent merged reflections ($R_{int} = 0.022$) converged at $wR_2(F^2) = 0.088$ for all data; $R_1(F) = 0.034$ for 5898 observed data [$I > 2\sigma(I)$].

CCDC reference numbers 167467–167471.

See http://www.rsc.org/suppdata/dt/b1/b103547a/ for crystallographic data in CIF or other electronic format.

Characterization of 1–5

(a) $Pd_{16}(CO)_{13}(PMe_3)_9$ 1. Elemental analysis was performed by Desert Analytics (Tucson, AZ). Calculated values are for $[Pd_{16}(CO)_{13}(PMe_3)_9]\cdot 2C_4H_8O$ (FW = 3013.55). Calc. (found): Pd, 58.80 (59.72); Ni, 0.00 (0.10); C, 19.91 (19.81); H, 3.38 (3.23); P, 9.63 (9.29)%.

An IR spectrum of **1** in THF (CaF_2 cell), exhibited bridging carbonyl bands at 1870vs, 1835vs, 1762w (sh), 1747m, 1725w, 1668m cm^{-1}.

Cyclic voltammograms of **1** in THF showed no reductions out to −2.8 V and no oxidations out to +1.0 V. A ^{1}H NMR spectrum of **1** in acetone-d_6 at room temperature displayed three doublets at δ 1.42 ($^2J_{P-H} = 7.88$ Hz), 1.30 ($^2J_{P-H} = 7.88$ Hz) and 1.10 ($^2J_{P-H} = 8.37$ Hz) with intensity ratios of 1 : 1 : 1. The first two doublets with the same J_{P-H} were assigned to the protons of the PMe_3 groups of the independent P(1) and P(2) atoms attached to the Pd atoms on the icosahedral surface; the other doublet at δ 1.10 was assigned to the protons of the remaining PMe_3 groups of P(3) and its two symmetry-related atoms. All other proton signals were due to the solvent. No evidence of signals due to hydrido-like protons was observed (from δ 9.0 to −30.0). A ^{31}P{^{1}H} NMR spectrum of **1** exhibited resonances with analogous intensities at δ −12.22 (s), −13.18 (d, $J_{P-P} = 84.0$ Hz) and −24.28 (d, $J_{P-P} = 80.0$ Hz). The singlet resonance was assigned to the three phosphorus atoms of P(3) type, and the doublets to phosphorus atoms of P(1) and P(2) types due to their positions in the molecule (*i.e.*, attached to the two opposite faces of an icosahedron) which allow a through-bond coupling between them. A singlet at δ −34.42 was attributed to a metallophosphine product of the decomposition of **1** in solvent. A ^{13}C{^{1}H} NMR spectrum of **1** exhibited a multiplet (due to an overlap of two doublets) at δ 15.78 and a doublet at δ 14.76 ($^1J_{C-P} = 74.5$ Hz) with an intensity ratio of 2 : 1 for C atoms on the PMe_3 groups of the three different types. Resonances due to the carbonyl carbon atoms were not observed in the spectrum.

(b) $Pd_{35}(CO)_{23}(PMe_3)_{15}$ 2. Elemental analysis was performed by Desert Analytics (Tucson, AZ). Calculated values are for $[Pd_{35}(CO)_{23}(PMe_3)_{15}]\cdot C_4H_8O$ (FW = 5581.43). Calc. (found): Pd, 66.72 (68.12); Ni, 0.00 (<0.10, non-detectable); C, 15.49 (16.11); H, 2.59 (2.63); P, 8.32 (8.51)%.

An IR spectrum of **2** (THF, CaF_2) exhibited bridging carbonyl bands at 1862s, 1739w, br and 1653w, br cm^{-1}. Small shoulders were observed at 1837, 1822 and 1800 cm^{-1}.

Cyclic voltammograms of **2** in THF showed no reduction waves out to −2.8 V and no oxidation waves out to +1.0 V. A ^{1}H NMR spectrum (500 MHz, THF-d_8, 23 °C) displayed four doublets at δ 1.48 ($^2J_{P-H} = 8.69$ Hz), 1.34 ($^2J_{P-H} = 12.92$ Hz), 1.30 ($^2J_{P-H} = 8.92$ Hz) and 1.24 ($^2J_{P-H} = 8.91$ Hz) with intensity ratios of 1 : 2 : 1 : 1. Under pseudo threefold molecular symmetry, five kinds of protons should be observed with the same intensity. The doublet at δ 1.34 reflects that two kinds of protons have similar environments; these were assigned to the protons on the PMe_3 ligands that are attached to Pd atoms on the surface of the two face-fused icosahedra. The other three doublets were assigned to the protons of the PMe_3 ligands attached to the three different types of capping Pd atoms. A small doublet observed at δ 1.06 ($J = 6.24$ Hz) is presumed to arise from the decomposition of **2** in the solvent. All other proton signals are due to the solvent. A ^{31}P{^{1}H} NMR spectrum of **2** exhibited resonances at δ +31.3 (s), −24.4 (s), −25.0 (d, $J_{P-P} = 29.0$ Hz) and −37.1 (d, $J_{P-P} = 33.0$ Hz) with approximate intensity ratios of 2 : 1 : 1 : 1. The first singlet, being twice the intensity of those of the other resonances, was assigned to the six PMe_3 groups, P(n) (where n = 1–6), attached to the Pd atoms on the surfaces of the face-fused icosahedra. The two doublets were assigned to two different kinds of three PMe_3 phosphorus atoms [*viz.*, P(7), P(8), P(9) and P(13), P(14), P(15)] which have P–P coupling. The doublet at δ −25.0, which possessed broad peaks, was assigned to the three PMe_3 phosphorus atoms [P(13), P(14), P(15)], based upon the presumption that the broadening is due to their weak-far coupling with P(10), P(11) and P(12), which appeared as a singlet at δ −24.4. A ^{13}C NMR spectrum surprisingly showed no resonances, even for the C atoms of PMe_3 ligands, except for those readily attributed to the solvent.

(c)$Pd_{39}(CO)_{23}(PMe_3)_{16}$ 3. Elemental analysis was performed by Desert Analytics (Tucson, AZ). Calc. for $[Pd_{39}(CO)_{23}(PMe_3)_{16}]\cdot 2Pri_2O$ (FW = 6216.45). Calc. (found): Pd, 66.76 (67.47); Ni, 0.00 (<0.15); C, 16.04 (15.97); H, 2.79 (2.77); P, 7.97 (7.65)%.

An IR spectrum of **3** (THF, CaF_2 cell) exhibited bridging carbonyl bands at 1843s, 1821s and 1795 (sh) cm^{-1}. Cyclic voltammograms of **3** in THF showed no reductions out to −2.8 V and no oxidations out to +1.0 V. A ^{1}H NMR spectrum of **3** in THF-d_8 at room temperature displayed two doublets with an intensity ratio of 4 : 1 at δ 1.34 ($^2J_{P-H} = 14.09$ Hz)

assigned to protons of PMe_3 ligands, and at δ 0.10 ($^2J_{P-H}$ = 10.56 Hz) due to an unknown species. All other proton signals were due to the solvent. No resonances ascribable to hydrido-like protons were detected from δ 9.0 to −30.0. A $^{31}P\{^1H\}$ NMR spectrum of **3** consisted of one resonance at δ 30.92 at room temperature. Even on cooling the sample to −60 °C, this resonance was not resolved into components. This indicates that the phosphine ligands in **3** are fluxional and are undergoing rearrangenent processes with low activation energies. None of the methyl ^{13}C resonances in **3** could be observed in a ^{13}C NMR spectrum, as was also found for $Pd_{35}(CO)_{23}(PMe_3)_{15}$.

(d) $Pd_{59}(CO)_{32}(PMe_3)_{21}$ 4. Elemental analysis was performed by Desert Analytics (Tucson, AZ). Calc. for $[Pd_{59}(CO)_{32}(PMe_3)_{21}]\cdot 3Me_2CO\cdot 1.5Pri_2O\cdot 2C_6H_{14}$: (FW = 9271.32). Calc. (found): Pd, 67.72 (67.59); Ni, 0.00 (0.16); C, 16.19 (16.29); H, 2.79 (2.80)%.

An IR spectrum of **4** (THF, CaF_2), exhibited bridging carbonyl bands at 1848br, 1820 (sh), 1739w, and 1653w cm^{-1}.

A ^1H NMR spectrum of **4** (THF-d_8 at room temperature) displayed two doublets at δ 1.34 ($^2J_{P-H}$ = 12.91 Hz), assigned to protons of PMe_3 ligands, and at δ 0.10 ($^2J_{P-H}$ = 9.30 Hz) due to unknown species, with intensity ratio of 2 : 1. All other proton signals were due to the solvent. No resonances characteristic of hydrido-like protons were found from δ 9.0 to −30.0. A $^{31}P\{^1H\}$ NMR spectrum of **4** consisted of one resonance at δ 31.30 at room temperature and at −60 °C. This indicates that phosphine ligands in **4** are highly fluxional and are undergoing rearrangement processes with low activation energies. Similar to $Pd_{35}(CO)_{23}(PMe_3)_{15}$ and $Pd_{39}(CO)_{23}(PMe_3)_{16}$, no ^{13}C resonances were observed in a ^{13}C NMR spectrum.

(e) $Pd_{29}Ni_3(CO)_{22}(PMe_3)_{13}$ 5. An IR spectrum of **5** in THF (CaF_2 cell), exhibited bridging carbonyl bands at 1859s, 1796w, 1755w br, and 1660w br, cm^{-1}. The observation that these frequencies are within the carbonyl absorption domain of both doubly and triply bridging COs (but not of terminal COs) is completely consist with the crystallographically determined molecular structure of **5** having only edge- and face-connected carbonyl ligands.

Acknowledgements

This research was supported by the National Science Foundation. Departmental purchase of the CCD area detector system in 1995 was made possible by funds from the NSF (Grant CHE-9310428) and the UW-Madison Graduate School and Chemistry Department. We are most grateful to Dr Douglas Powell (UW-Madison) for helpful crystallographic assistance. Color figures were prepared with Crystal Maker, Interactive Crystallography (version 4), David C. Palmer (P.O. Box 183 Bicester, Oxfordshire, UK 0XG 7BS).

References

1 P. Chini, *Gazz. Chim. Ital.*, 1979, **109**, 225.
2 G. Longoni and M. C. Iapalucci, in *Clusters and Colloids: From Theory to Applications*, ed. G. Schmid, VCH Publishers: Inc., New York, NY, 1994, pp. 91–177 and references therein; A. Ceriotti, R. D. Pergola and L. Garlaschelli, in *Physics and Chemistry of Metal Cluster Compounds*, ed. L. J. de Jongh, Kluwer Academic Publishers, The Netherlands, 1994, ch. 2, pp. 41–106 and references therein; K. C. C. Kharas and L. F. Dahl, *Adv. Chem. Phys.*, 1988, **70** (part 2), pp. 1–43 and references therein.
3 $[HNi_{34}C_4(CO)_{38}]^{5-}$, $[Ni_{35}(CO)_{39}C_4]^{6-}$: A. Ceriotti, A. Fait, G. Longoni, G. Piro, L. Resconi, F. Demartin, M. Manassero, N. Masciocchi and M. Sansoni, *J. Am. Chem. Soc.*, 1986, **108**, 5370; $[HNi_{38}(CO)_{42}C_6]^{5-}$: A. Ceriotti, A. Fait, G. Longoni, G. Piro, F. Demartin, M. Manassero, N. Masciocchi and M. Sansoni, *J. Am. Chem. Soc.*, 1986, **108**, 8091; $[H_2Ni_{38}Pt_6(CO)_{48}]^{4-}$, $[HNi_{38}Pt_6(CO)_{44}]^{5-}$: A. Ceriotti, F. Demartin, G. Longoni, M. Manassero, M. Maichionna, G. Piva and M. Sansoni, *Angew. Chem., Int. Ed. Engl.*, 1985, **24**, 697; $[Ni_{38}Pt_6(CO)_{44}]^{6-}$: J. M. Bemis and L. F. Dahl, unpublished work; $[Pt_{44}(CO)_{47}]^{4-}$, $[Pt_{50}(CO)_{48}]^{4-}$: G. J. Lewis, R. K. Hayashi and L. F. Dahl, unpublished work (see: p. 6166, in J. D. Roth, G. J. Lewis, L. K. Safford, X. Jiang, L. F. Dahl and M. J. Weaver, *J. Am. Chem. Soc.*, 1992, **114**, 6159).
4 The so-called "non-classical" square-planar $[M(CO)_4]^{2+}$ dications (M = Pd, Pt)[5] isolated as white, thermally stable, crytalline salts are excluded. These dications are members of a small class of homoleptic noble-gas carbonyl cations that display exceptionally high carbonyl stretching frequencies.[6].
5 G. Hwang, C. Wang, F. Aubke, H. Willner and M. Bodenbinder, *Can. J. Chem.*, 1993, **71**, 1532; L. Weber, *Angew. Chem., Int. Ed. Engl.*, 1994, **33**, 1077.
6 F. Aubke and C. Wang, *Coord. Chem. Rev.*, 1994, **137**, 483 and references therein S. H. Strauss, *J. Chem. Soc., Dalton Trans.*, 2000, 1 and references therein; A. S. Goldman and K. Krogh-Jespersen, *J. Am. Chem. Soc.*, 1996, **118**, 12159.
7 (*a*) T. A. Stromnova and I. I. Moiseev, *Russ. Chem. Rev.*, 1998, **67**, 485 and references therein; (*b*) K. R. Dixon and A. C. Dixon, in *Comprehensive Organometallic Chemistry II*, ed. R. J. Puddephatt, Pergamon, London, 1995, vol. 9, p. 198 and references therein; (*c*) Y. Y. Yeo, L. Vattuone and D. A. King, *J. Chem. Phys.*, 1997, **106**, 1990 and references therein; (*d*) V. A. Spasov and K. M. Ervin, *J. Chem. Phys.*, 1998, **109**, 5344.
8 (*a*) A. Misono, Y. Uchida, M. Hidai and K. Kudo, *J. Organomet. Chem.*, 1969, **20**, P7; (*b*) K. Kudo, M. Hidai and Y. Uchida, *J. Organomet. Chem.*, 1971, **33**, 393; (*c*) M. Hidai, K. Kokura and Y. Uchida, *J. Organomet. Chem.*, 1973, **52**, 431; (*d*) E. G. Mednikov, N. K. Eremenko, Yu. L. Slovokhotov, Yu. T. Struchkov and S. P. Gubin, *Koord. Khim.*, 1987, **13**, 979.
9 E. G. Mednikov, N. K. Eremenko, Yu. L. Slovokhotov and Yu. T. Struchkov, *J. Organomet. Chem.*, 1983, **258**, 247.
10 E. G. Mednikov, N. K. Eremenko, S. P. Gubin, Yu. L. Slovokhotov and Yu. T. Struchkov, *J. Organomet. Chem.*, 1982, **239**, 401.
11 E. G. Mednikov, Yu. T. Struchkov and Yu. L. Slovokhotov, *J. Organomet. Chem.*, 1998, **566**, 15.
12 E. G. Mednikov, Yu. L. Slovokhotov and Yu. T. Struchkov, *Metalloorg. Khim.*, 1991, **4**, 123.
13 E. G. Mednikov, N. K. Eremenko, Yu. L. Slovokhotov and Yu. T. Struchkov, *J. Organomet. Chem.*, 1986, **301**, C35; E. G. Mednikov, *Organomet. Chem. (USSR) (Engl. Transl.)*, 1991, **4**, 433.
14 E. G. Mednikov, N. K. Eremenko, Yu. L. Slovokhotov and Yu. T. Struchkov, *Zh. Vses. Khim. Ova im. D. I. Mendeleeva*, 1987, **32**, 101 (in Russian); E. G. Mednikov, *Russ. Chem. Bull.*, 1993, **42**, 1242.
15 E. G. Mednikov and N. I. Kanteeva, *Russ. Chem. Bull.*, 1995, **44**, 163.
16 E. G. Mednikov, N. K. Eremenko, Yu. L. Slovokhotov and Yu. T. Struchkov, *J. Chem. Soc., Chem. Commun.*, 1987, 218.
17 N. K. Eremenko and S. P. Gubin, *Pure Appl. Chem.*, 1990, **62**, 1179; A. D. Burrows and D. M. P. Mingos, *Transition Met. Chem.*, 1993, **18**, 129; R. B. King, *Gazz. Chim. Ital.*, 1992, **122**, 383.
18 N. T. Tran, D. R. Powell and L. F. Dahl, *Angew. Chem., Int. Ed.*, 2000, **39**, 4121.
19 These ligand-stabilized non-carbonyl clusters are members of a series of idealized spherically-shaped nanocluster molecules denoted as *full-shell* clusters. Their metal-atom cores arise from a central atom being completely surrounded by one or more close-packed cuboctahedral or icosahedral shells such that each inner shell is encapsulated by the adjacent outer shell. A given n^{th} shell consists of $10n^2 + 2$ atoms. These *n*-shell M_N cores thereby possess so-called magic numbers of *N* atoms – ones with *N* values of 13, 55, 147, 309, 561 *etc.* for corresponding *n*-shell clusters with *n* = 1, 2, 3, 4, 5, *etc.* The non-isolation (to date) of crystalline samples of any of these *full-shell* metal-ligated clusters (for X-ray diffraction analysis) has been attributed to packed solids of these macromolecules having only short-range order; therefore, their idealized formulations are mainly based upon high-resolution electron microscopy and mass spectra.
20 M. N. Vargaftik, V. P. Zagorodnikov, I. P. Stolyarov, I. I. Moiseev, V. A. Likholobov, D. I. Kochubey, A. L. Chuvilin, V. I. Zaikovsky, K. I. Zamaraev and G. I. Timofeeva, *J. Chem. Soc., Chem. Commun.*, 1985, 937; M. N. Vargaftik, I. I. Moiseev, D. I. Kochubey and K. I. Zamaraev, *Faraday Discuss.*, 1991, **92**, 13; I. I. Moiseev and M. N. Vargaftik, *Catalysis with Palladium Clusters, in Catalysis by Di- and Polynuclear Metal Cluster Compounds*, eds. R. D. Adams and F. A. Cotton, Wiley-VCH, Inc:, New York, 1998, pp. 395–442; T. A. Stromnova and I. I. Moiseev, *Russ. Chem. Rev.*, 1998, **67**, 485.
21 G. Schmid, *Polyhedron*, 1988, **7**, 2321; G. Schmid, *Chem. Rev.*, 1992, 1709; G. Schmid, in *Physics and Chemistry of Metal Cluster Compounds*, ed. L. J. de Jongh, Kluwer Academic Publishers, The

Netherlands, 1994, ch. 3, pp 107–134; and references therein; G. Schmid, in *Clusters and Colloids: From Theory to Applications*, ed. G. Schmid, VCH Publishers: Inc., New York, NY, 1994, pp. 178–211 and references therein.
22 G. Schmid, M. Harms, J.-O. Malm, J.-O. Bovin, J. van Ruitenbeck, H. W. Zandbergen and W. T. Fu, *J. Am. Chem. Soc.*, 1993, **115**, 2046.
23 C. Amiens, D. de Caro, B. Chaudret, J. S. Bradley, R. Mazel and C. Roucau, *J. Am. Chem. Soc.*, 1993, **115**, 11638.
24 (*a*) J. W. Bacon, Ph.D. Thesis, University of Wisconsin-Madison, 1994; (*b*) Crystal data for crystal **A**: pseudo-orthorhombic with $a = 18.960$ $b = 18.319$ $c = 30.016$ Å $V = 16{,}116$ Å^3; actually has monoclinic unit cell ($\beta \approx 90°$ with $P2_1/n$, $Z = 4$) that is twinned by "merohedry" with *hkl*, $\bar{h}kl$ data superimposed by (100) twin plane. Crystal structure determination (direct methods/Fourier difference maps) clearly revealed the 30-atom metal-core geometry. An assumed average volume of 19 Å^3 per non-hydrogen atom, found in other high-nuclearity metal carbonyl clusters, gives 16,116 Å^3/19 Å^3 = 849 non-hydrogen atoms per unit cell or 212 independent non-hydrogen atoms in the asymmetric unit of $P2_1/n$. Tentative formulation of $[PPh_4]_4[Pd_{30-x}Ni_x(CO)_y]\cdot 1$–3 solvent molecules (where $x \approx 13$; $y \approx 36$ based upon related clusters) gives 4 × 25 atoms (cations) +102 atoms (anion) +10 atoms (solvent) = 212 total non-hydrogen atoms in the asymmetric unit.
25 N. T. Tran, M. Kawano, D. R. Powell and L. F. Dahl, *J. Am. Chem. Soc.*, 1998, **120**, 10986.
26 C. A. Tolman, *Chem. Rev.*, 1977, **77**, 313; D. M. P. Mingos, *Inorg. Chem.*, 1982, **21**, 466.
27 A regular 13-atom centered icosahedron may be considered as 20 identical (slightly deformed) fcc tetrahedra that share a common vertex (*i.e.*, corresponding to the centered atom) and are joined to one another through adjacent shared faces. Based upon a hard-sphere icosahedral model, Mackay[28] predicted that a radial compression would occur for each tetrahedron in which the three radial tetrahedral edges would be contracted by *ca.* 5% relative to the three tangential tetrahedral edges of the triangular surface (111) face.
28 A. L. Mackay, *Acta Crystallogr.*, 1962, **15**, 916; S. Ino, *J. Phys. Soc. Jpn.*, 1966, **21**, 346; J. Farges, M. F. de Feraudy, B. Raoult and G. Torchet, *Acta Crystallogr., Sect. A*, 1982, **38**, 656.
29 R. C. B. Copley, C. M. Hill and D. M. P. Mingos, *J. Cluster Sci.*, 1995, **6**, 71.
30 J. Donahue, *The Structure of the Elements*, John Wiley and Sons, Inc., New York, 1974, p. 216.
31 (*a*) D. M. P. Mingos, *J. Chem. Soc., Chem. Commun.*, 1983, 706; (*b*) D. M. P. Mingos, *J. Chem. Soc., Chem. Commun.*, 1983, 1352; (*c*) D. M. P. Mingos, *Acc. Chem. Res.*, 1984, **17**, 311; (*d*) D. M. P. Mingos, *Polyhedron*, 1984, **3**, 1289; (*e*) K. P. Hall and D. M. P. Mingos, *Prog. Inorg. Chem.*, 1984, **32**, 237; (*f*) D. M. P. Mingos and R. L. Johnson, *J. Organomet. Chem.*, 1985, **280**, 419; (*g*) D. M. P. Mingos and L. Zhenyang, *J. Chem. Soc., Dalton Trans.*, 1988, 1657 and references therein; (*h*) D. M. P. Mingos and A. P. May, in *The Chemistry of Metal Cluster Complexes*, eds. D. F. Shriver, H. D. Kaesz and R. D. Adams, VCH Publishers, New York, 1990, ch. 2, pp. 11–119; (*i*) D. M. P. Mingos and D. J. Wales, *Introduction to Cluster Chemistry*, Prentice Hall, Old Tappan, NJ, 1990; (*j*) D. M. P. Mingos and M. J. Watson, *Adv. Inorg. Chem.*, 1992, **39**, 327.
32 The observed electron count of 170 for an all-metal carbonyl icosahedral cage that is either empty or one that contains a non-metal centered atom is equivalent to a skeletal electron-pair *B* value of 13 (*i.e.* 170 − 144 = 26 skeletal bonding electrons, where 144 is the number of external electrons occupying the 72 non-skeletal external orbitals (12 × 6) of the 12 transition-metal cage atoms; each transition metal atom in both models is presumed to possess three skeletal and six non-skeletal orbitals). Although there are no examples of a *non-centered* all transition-metal cage, examples of the latter case (*i.e.* ones with centered main-group atoms) are the Sb-centered $[(\mu_{12}\text{-Sb})Rh_{12}(CO)_{27}]^{3-}$ trianion[33] and the E-centered $[(\mu_{12}\text{-E})Ni_{12}(CO)_{22}]^{2-}$ dianions (E = Ge, Sn).[34] However, there are a considerable number of known non-centered icosahedral cages containing both transition-metal and main-group atoms in which electronically equivalent (isolobal) main-group fragments are formally substituted for metal carbonyl fragments; one prominent example is the homologous $[Ni_{12-x}(PMe)_x(CO)_{24-3x}]^{2-}$ series ($x = 2$, 3, 4) containing empty $Ni_{12-x}P_x$ icosahedral cages related by the formal replacement of $Ni(CO)_3$ fragments with isolobal PMe fragments.[35] The observed electron counts of 150 for $x = 2$, 140 for $x = 3$, and 130 for $x = 4$ are in agreement with the number of skeletal electron pairs (*i.e.* the *B* value) remaining at 13 for each of the three clusters but with the electron count decreasing from 170 by units of 10 for each replacement of a $Ni(CO)_3$ fragment by an isolobal PMe fragment; this uniform decrease in electron count occurs because each main-group P atom possesses no d valence electrons. Of prime interest is that the current electron-counting models[31,39] do not work when applied to icosahedral cage clusters containing centered (interstitial) $3d^{10}$ Ni atoms. Thus, in sharp contrast to the exact agreement of the predicted electron count with the observed electron count for the non-centered (empty) Ni_8Te_4 cage in $[Ni_8Te_4(CO)_{12}]^{2-}$ (130 e$^-$),[36] the observed electron counts for the Ni-centered $Ni_{10}E_2$ cages in $[(\mu_{12}\text{-Ni})Ni_{10}E_2(CO)_{18}]^{2-}$ (E = Se, Te; 150 e$^-$)[36] and for the Ni-centered Ni_9E_3 cage in $[(\mu_{12}\text{-Ni})Ni_9Te_3(CO)_{15}]^{2-}$ (160 e$^-$)[36] are 10 electrons higher than those predicted by the Mingos model; likewise, the observed electron count for the $Ni_{10}Sn_2$ cages in $[(\mu_{12}\text{-Ni})\text{-}Ni_{10}(SnR)_2(CO)_{18}]^{2-}$ (R = Bu^n, Me; 158 e$^-$)[37] is 8 electrons in excess of the predicted number. The same problem was encountered for the Ni-centered $Ni_{10}Sb_2$ cage in the $[(\mu_{12}\text{-Ni})Ni_{10}(SbNi(CO)_3)_2(CO)_{18}]^{n-}$ anions ($n = 2$, 3, 4 with 158, 159, 160 e$^-$, respectively), for which observed electron counts are 8–10 electrons higher than the predicted values.[38] Comparative structural-bonding analyses[36–38] of closely related clusters with and without Ni(i)-centered atoms were found to be consistent with the view that the interstitial $3d^{10}$ Ni(i)-centered atom contributes its empty valence 4s, 4p AOs (to form four strongly bonding radial skeletal MOs) but no "net bonding" 3d skeletal electron pairs in stabilizing the cage geometries (*i.e.* only weak radial interactions occur between the filled 3d Ni(i) AOs and appropriate cage orbitals). A similar explanation put forth by the Italian scientists[38a] was subsequently supported by EHMO computations[38b] of hypothetical icosahedral systems.
33 J. L. Vidal and J. M. Troup, *J. Organomet. Chem.*, 1981, **213**, 351; B. T. Heaton, L. Strona, R. D. Pergola, J. L. Vidal and R. C. Schoening, *J. Chem. Soc., Dalton Trans.*, 1983, 1941.
34 A. Ceriotti, F. Demartin, B. T. Heaton, P. Ingallina, G. Longoni, M. Manassero, M. Marchionna and N. Masciocchi, *J. Chem. Soc., Chem. Commun.*, 1989, 786.
35 D. F. Rieck, J. A. Gavney, Jr., R. L. Norman, R. K. Hayashi and L. F. Dahl, *J. Am. Chem. Soc.*, 1992, **114**, 10369 and references therein.
36 A. J. Kahaian, J. B. Thoden and L. F. Dahl, *J. Chem. Soc., Chem. Commun.*, 1992, 353.
37 J. P. Zebrowski, R. K. Hayashi and L. F. Dahl, *J. Am. Chem. Soc.*, 1993, **115**, 1142 and references therein.
38 (*a*) V. G. Albano, F. Demartin, M. C. Iapalucci, G. Longoni, A. Sironi and V. Zanotti, *J. Chem. Soc., Chem. Commun.*, 1990, 547; (*b*) V. G. Albano, F. Demartin, M. C. Iapalucci, F. Laschi, G. Longoni, A. Sironi and P. Zanello, *J. Chem. Soc., Dalton Trans.*, 1991, 739.
39 B. K. Teo and H. Zhang, *Inorg. Chim. Acta*, 1988, **144**, 173; B. K. Teo and H. Zhang, *Polyhedron*, 1990, **9**, 1985.
40 (*a*) C. E. Briant, B. R. C. Theobald, J. W. White, L. K. Bell, D. M. P. Mingos and A. J. Welch, *J. Chem. Soc., Chem. Commun.*, 1981, 201; (*b*) M. Lapp and J. Strähle, *Z. Naturforsch., Teil B*, 1995, **50**, 1369; (*c*) M. Laupp and J. Strähle, *Angew. Chem., Int. Ed. Engl.*, 1994, **33**, 207; (*d*) R. C. B. Copley and D. M. P. Mingos, *J. Chem. Soc., Dalton Trans.*, 1992, 1755; (*e*) B. K. Teo, H. Dang and H. Zhang; as quoted in H. Zhang and B. K. Teo, *Inorg. Chim. Acta*, 1997, **265**, 213; (*f*) B. K. Teo and H. Zhang, *J. Organomet. Chem.*, 2000, **614**, 66.
41 N. Rösch, A. Görling, D. E. Ellis and H. Schmidbaur, *Angew. Chem. Int. Ed. Engl.*, 1989, **28**, 1357; P. Pyykkö, *Chem. Rev.*, 1988, **88**, 593; V. Bonacic-Koutecky, P. Fantucci and J. Koutecky, *Chem. Rev.*, 1991, **91**, 1035; K. S. Pitzer, *Acc. Chem. Res.*, 1979, **12**, 271; K. Balasubramanian, *J. Phys. Chem.*, 1989, **93**, 6585; P. Schwerdtfeger and P. D. W. Boyd, *Inorg. Chem.*, 1992, **31**, 327; P. Pyykkö and Y. Zhao, *Angew. Chem., Int. Ed. Engl.*, 1991, **30**, 604.
42 (*a*) B. K. Teo, H. Zhang and X. Shi, *J. Am. Chem. Soc.*, 1990, **112**, 8552; (*b*) B. K. Teo and H. Zhang, *Proc. Natl. Acad. Sci. USA*, 1991, **88**, 5067 and references therein; (*c*) B. K. Teo and H. Zhang, *Coord. Chem. Rev.*, 1995, **143**, 611; (*d*) H. Zhang and B. K. Teo, *Inorg. Chim. Acta*, 1997, **265**, 213; (*e*) B. K. Teo, A. Strizhev, R. Elber and H. Zhang, *Inorg. Chem.*, 1998, **37**, 2482.
43 B. K. Teo, H. Zhang and X. Shi, *Inorg. Chem.*, 1990, **29**, 2083.
44 Of interest is that the metal framework in the corresponding triphenylphosphine analogue was found to exist in the solid state as two distinct rotamers for different counter ions: namely, $[Au_{13}Ag_{12}(PPh_3)_{10}Br_2(\mu_2\text{-Br})_4(\mu_4\text{-Br})_2]^+$ (as the $[SbF_6]^-$ salt)[45] with a ses configuration and $[Au_{13}Ag_{12}(PPh_3)_{10}Br_2(\mu_2\text{-Br})_4(\mu_4\text{-Br})_2]^+$ (as the $[Br]^-$ salt) with a sss configuration.[46]
45 B. K. Teo, X. Shi and H. Zhang, *J. Am. Chem. Soc.*, 1991, **113**, 4329.
46 B. K. Teo, X. Shi and H. Zhang, *J. Chem. Soc., Chem. Commun.*, 1992, 1195.
47 B. K. Teo and H. Zhang, *Inorg. Chem.*, 1991, **30**, 3115.
48 B. K. Teo, H. Dang, C. F. Campana and H. Zhang, *Polyhedron*, 1998, **17**, 617.

49 B. K. Teo, M. Hong, H. Zhang, D. Huang and X. Shi, *J. Chem. Soc., Chem. Commun.*, 1988, 204; B. K. Teo, H. Zhang and X. Shi, *J. Am. Chem. Soc.*, 1990, **112**, 8552.
50 Z. Lin, R. P. F. Kanters and D. M. P. Mingos, *Inorg. Chem.*, 1991, **30**, 91.
51 (*a*) A. J. W. Johnson, B. Spencer and L. F. Dahl, *Inorg. Chim. Acta*, 1994, **227**, 269 and references therein; (*b*) R. G. Woolley, *Inorg. Chem.*, 1985, **24**, 3525.
52 A. Ceriotti, P. Chini, R. D. Pergola and G. Longoni, *Inorg. Chem.*, 1983, **22**, 1595.
53 E. G. Mednikov, N. K. Eremenko, V. A. Mikhailov, S. P. Gubin, Yu. L. Slovokhotov and Yu. T. Struchkov, *J. Chem. Soc., Chem. Commun.*, 1981, 989.
54 C. L. Briant and J. Burton, *Phys. Status Solidi B*, 1978, **85**, 393; F. Machizaud, F. A. Kuhnast and J. Flechon, *Ann. Chim.*, 1978, **3**, 177.
55 A. Renou and M. Gillet, *Surf. Sci.*, 1981, **106**, 27 and references therein; N. Toshima and T. Yonezawa, *New J. Chem.*, 1998, **22**, 1179 and references therein.
56 R. B. King, *Inorg. Chim. Acta*, 1992, **198**, 841.
57 M. Tillard-Charbonnel, A. Manteghetti and C. Belin, *Inorg. Chem.*, 2000, **39**, 1684 and references therein.
58 J. H. Enemark, L. B. Friedman and W. N. Lipscomb, *Inorg. Chem.*, 1966, **5**, 2165.
59 Y. M. Cheek, N. N. Greenwood, J. D. Kennedy and W. S. McDonald, *J. Chem. Soc., Chem. Commun.*, 1982, 80.
60 (*a*) M. Vlasse, R. Naslain, J. S. Kasper and K. Ploog, *J. Solid State Chem.*, 1979, **28**, 289; (*b*) C. Belin, *J. Solid State Chem.*, 1983, **50**, 225; (*c*) M. Charbonnel and C. Belin, *Nouv. J. Chim.*, 1984, **10**, 595; (*d*) M. Charbonnel and C. Belin, *J. Solid State Chem.*, 1987, **67**, 210.
61 J. K. Burdett and E. Canadell, *J. Am. Chem. Soc.*, 1990, **112**, 7207 and references therein; J. K. Burdett and E. Canadell, *Inorg. Chem.*, 1991, **30**, 1991.
62 Noteworthy is that the electron-counting models of Mingos,[31] Teo/Zhang,[39] and King,[63] have successfully correlated the geometries of condensed transition-metal polyhedral clusters with their observed numbers of cluster valence electrons. However, Burdett and Canadell[61] showed in general that these models did not work when applied to solid-fused (Group 13) boron or gallium systems, and consequently they developed more complex electron-counting rules to cover fused boride and gallide polyhedra in a number of solid-state structures.
63 R. B. King, *Inorg. Chim. Acta*, 1991, **181**, 217 and references therein.
64 N. K. Eremenko, E. G. Mednikov and S. S. Kurasov, *Russ. Chem. Rev.*, 1985, **54**, 394.
65 M. R. Hoare and P. Pal, *Adv. Phys.*, 1971, **20**, 161; M. R. Hoare and P. Pal, *Adv. Phys.*, 1975, **24**, 645; C. L. Briant and J. J. Burton, *Phys. Status Solidi B*, 1978, **85**, 393.
66 J. Farges, M. F. de Feraudy, B. Raoult and G. Torchet, *Surf. Sci.*, 1985, **156**, 370; J. Farges, M. F. de Feraudy, B. Raoult and G. Torchet, *Adv. Chem. Phys.*, 1988, **70**, 45.
67 I. A. Harris, R. S. Kidwell and J. A. Northby, *Phys. Rev. Lett.*, 1984, **53**, 2390.
68 J. C. Calabrese, L. F. Dahl, A. Cavalieri, P. Chini, G. Longoni and S. Martinengo, *J. Am. Chem. Soc.*, 1974, **96**, 2616; G. Longoni, P. Chini and A. Cavalieri, *Inorg. Chem.*, 1976, **15**, 3025; A. Ceriotti, G. Longoni and G. Piva, *Inorg. Synth.*, 1989, **26**, 312.
69 M. Kawano, J. W. Bacon, C. F. Campana, B. E. Winger, J. D. Dudek, S. A. Sirchio, S. L. Scruggs, U. Geiser and L. F. Dahl, *Inorg. Chem.*, 2001, **40**, 2554.
70 A. J. Amoroso, L. H. Gade, B. F. G. Johnson, J. Lewis, P. R. Raithby and W.-T. Wong, *Angew. Chem., Int. Ed. Engl.*, 1991, **30**, 107; L. H. Gade, B. F. G. Johnson, J. Lewis, M. J. McPartlin, H. R. Powell, P. R. Raithby and W.-T. Wong, *J. Chem. Soc., Dalton Trans.*, 1994, 521.
71 N. T. Tran, M. Kawano, D. R. Powell and L. F. Dahl, *J. Chem. Soc., Dalton Trans.*, 2000, 4138.